Structural Engineering and Mechanics, *Vol. 70, No. 6 (2019) 683-702*
DOI: https://doi.org/10.12989/sem.2019.70.6.683

Free vibration analysis of thick cylindrical MEE composite shells reinforced CNTs with temperature-dependent properties resting on viscoelastic foundation

Mehdi Mohammadimehr*[1], Ehsan Arshid[1], Seyed Mohammad Amin Rasti Alhosseini[1], Saeed Amir[1] and Mohammad Reza Ghorbanpour Arani[2]

[1]*Department of Solid Mechanics, Faculty of Mechanical Engineering, University of Kashan, Kashan, Iran*
[2]*Electrical Engineering Department, Amirkabir University of Technology, Tehran, Iran*

(Received February 3, 2019, Revised March 11, 2019, Accepted March 16, 2019)

Abstract. The present study aims to analyze the magneto-electro-elastic (MEE) vibration of a functionally graded carbon nanotubes reinforced composites (FG-CNTRC) cylindrical shell. Electro-magnetic loads are applied to the structure and it is located on an elastic foundation which is simulated by visco-Pasternak type. The properties of the nano-composite shell are assumed to be varied by temperature changes. The third-order shear deformation shells theory is used to describe the displacement components and Hamilton's principle is employed to derive the motion differential equations. To obtain the results, Navier's method is used as an analytical solution for simply supported boundary condition and the effect of different parameters such as temperature variations, orientation angle, volume fraction of CNTs, different types of elastic foundation and other prominent parameters on the natural frequencies of the structure are considered and discussed in details. Design more functional structures subjected to multi-physical fields is of applications of this study results.

Keywords: vibration analysis; third-order shear deformation theory; cylindrical shell; carbon nanotubes; electro-magnetic loads; Visco-Pasternak foundation

1. Introduction

Nowadays scientists are trying to find out new materials properties to use them in different structures to achieve the best results. Since the composite materials have great mechanical properties, they are used in engineering structures extensively. In recent decades, studies on reinforced composites which caused improvement in the mechanical behavior of the structures are developing. One of the best reinforcement materials used in reinforced composites is carbon nanotubes (CNTs). After detection of the CNTs in the 1990s by Iijima (1991) and by considering their significant properties by other researchers, CNTs reinforced composites (CNTRCs) are selected as one of the most valuable materials to use in the engineering structures. Very high elastic modulus and magnetic property are the main features of CNTs. It should be noted that CNTs are often used as the reinforcement of the polymeric composites and mechanical behavior of the reinforced composite are affected by their arrangement direction. Due to the mentioned properties of CNTRCs, they can be used in aerospace industries, electronic engineering and smart structures (Abdel-Rahman *et al*. 2002, Ashrafi *et al*. 2006).

In the last several years, various analyses of the structures had been investigated by many authors (Forsberg 1964, Hu 1964, Leissa 1973, Qatu 2002, Soedel 1983, Soedel 2004, Mohammadimehr and Shahedi 2017). Vibrational behavior of a thin cylindrical shell analyzed by Li (2006). Vibrations of orthotropic and laminated orthotropic cylindrical shells is presented by Das and Dong, respectively (1964, 1968). Ganesan and Sivasan (1990) researched about the vibration analysis of orthotropic shells with variable thickness. The vibration analysis of circular cylindrical shells of finite length is studied by Vronay and Smith (1970). Qatu (Qatu *et al*. 2010, Qatu 2004) researched about laminated composite shells and plates and their dynamic response. Liu *et al*. (2012) discussed orthotropic cylindrical shells and analyzed their vibrations. Also, many kinds of research about reinforced composite and size dependent effect have been done in the literature (Ghorbanpour Arani *et al*. 2016a, b, 2017a, 2108c, 2019, Mehar *et al*. 2017, Mohammadimehr and Rahmati 2013). Shen and Zhang (2010) studied about functionally graded (FG) CNTRC plates. They considered thermal buckling and post-buckling of them and assumed temperature variations affected on single-walled carbon nanotubes (SWCNTs) properties and achieved their results using multi-scale approach. Malekzadeh and Shojaee (2013) considered buckling of quadrilateral laminated plates with CNTRCs layers. Some researchers studied about size dependent effect as well as CNTRCs in their works (Mohammadimehr *et al*. 2010, 2014, 2015, 2016a,b,c,d, Ghorbanpour Arani *et al*. 2011a,b, Mohammadimehr and Mostafavifar 2016). They considered CNTRCs as face sheets in sandwich structures, considered their properties to be temperature-

*Corresponding author, Associate Professor
E-mail: mmohammadimehr@kashanu.ac.ir

ISSN: 1225-4568 (Print), 1598-6217 (Online)

dependent, studied about them in small scales and investigated their behaviors subjected to electric and magnetic fields and presented their findings and illustrated the effect of different parameters on the results. Effect of thermal environment on the dynamic response of CNTRCs plates is investigated by Wang and Shen (2011, 2012). They considered two patterns for CNTs distribution along the thickness of the plate and concluded that as the CNTs volume fraction increases, it leads the natural frequency to higher values. Shen and his co-authors presented their studies about post-buckling and nonlinear vibration of CNTRCs shells and panels (Shen 2011a,b, 2012, Shen and Xiang 2012, 2013). They investigated thermal and mechanical buckling and also the vibration of them. Aragh *et al*. (2012) analyzed vibration of continuously graded CNTs reinforced cylindrical panels for various boundary conditions using 2D generalized differential quadrature method (GDQM) solution method. Jam *et al*. (2012) employed 3D elasticity to analyze vibration of CNTRCs panels. They used the extended mixture rule to determine the effective properties values. The aspect ratio and waviness of CNTs are the most important parameters that they discussed about. Yas *et al*. (2013) presented a vibrational analysis using 3D elasticity about CNTRC panels and compared different patterns for distribution of CNTs in the panel. Shen and Xiang (2014) with regard to large amplitude deflection, considered vibration of CNTRCs cylindrical panels and used higher-order shear deformation theory (HSDT) to extract the motion equations. HSDT can be used for thick structures due to accounting the shear deformation effects. Therefore, the equations were governed based on it are more complex than other theories but the results are more accurate, too. One of the most popular types of HSDT is the third-order shear deformation theory (TSDT) which is also called Reddy's theory (Cong *et al*. 2018, Reddy 2004, Wattanasakulpong and Bui 2018). Also, other types of TSDT which are in refined forms are used recently by the researchers. A novel third-order shear deformation theory employed by Bui *et al*. (2016) to investigate the effect of high temperature on mechanical behaviors of FG plates. In another study, Vu *et al*. (2018) used a four-variable TSDT to consider bending, buckling and vibration behaviors of FG plates. A similar theory was employed by Do *et al*. (2017) to investigate the bending and buckling behaviors of a bi-directional FG plate. Yin *et al*. (2016b) analyzed buckling and free vibration of FG plates based on a refined TSDT which allowed them to account shear deformation effect without requiring any shear correction factors.

Moreover, in the case of the structures with crack or internal defects, some studies are done (Yu *et al*. 2016, Bhardwaj *et al*. 2015). According to the FSDT, effect of internal defects on the vibration and buckling behaviors of the FG imperfect plates considered by Yin *et al*. (2016a). They investigated effect of imperfection and other important parameters on the natural frequencies and critical buckling loads of the considered plate. Effect of crack length on the buckling load of a composite FG plate presented by Liu *et al*. (2015). They found that the crack causes degradation in stiffness of the structure and following it, the buckling load will strongly be affected. About small-scaled structures, Liu *et al*. (2017) considered the mechanical behaviors of a moderately thick micro plate based on FSDT. Liu *et al*. (2018) also presented an effective numerical model based on extended isogeometric analysis for assessment of vibration and buckling of FG micro plates with cracks. They captured the size effects using the modified couple stress theory. A computational approach for mechanical behavior of nanoplates presented Liu *et al*. (2019). They concluded that both microstructure and surface energy effects increase the rigidity of nanoplates.

Recently, mechanical analysis of the structures in multi-physical fields attracted the researchers. The most noted of them are electric and magnetic ones. Ansari and Gholami (2016) considered magneto-electro-thermo fields' effect on the vibration of rectangular nano plates. Similar effect but about buckling and vibration of FG cylindrical shells performed by Lang and Xuewu (2013). Magneto-electro-elastic (MEE) composite structures optimization investigated by Loja *et al*. (2014). They used differential evolution for their analysis. Razavi and Shooshtari (2015) discussed nonlinear vibration of MEE rectangular plates. Amir *et al*. (2018) presented vibration analysis of a thick sandwich plate with piezo-electro-magnetic face sheets subjected to pre electro-magnetic and mechanical pre loads. Also, analyze of CNTRCs subjected multi-physical loads have been done by some researchers. Ghorbanpour Arani *et al*. (2012) considered the effect of CNTs volume fraction on the behavior of smart composite cylinder. Alibeigloo (2014) investigated FG-CNTRC plate which was located between two piezoelectric layers as sensor and actuator. Dynamic stability of viscoelastic piezoelectric FG-CNTRC plate under multi-physical loadings studied by Mohammadimehr *et al*. (2017a). They considered multi-physical loadings and investigated the effect of surface stress and agglomeration of nanotubes. Nasihatgozar *et al*. (2016) discussed buckling of piezoelectric cylindrical CNTRCs panels and Mohammadimehr *et al*. (2018a) used high order sandwich panel theory to investigate MEE cylindrical panel vibrations which was integrated with FG-CNTRCs layers. They considered the properties temperature dependent and discussed various circuit boundary conditions. Vibration analysis of MEE cylindrical CNTRCs panel developed by Mohammadimehr *et al*. (2018b). They considered open and closed circuits conditions and various distributions of CNTs in their analysis.

By reviewing the literature it can be seen that up to date there are no researches about MEE analysis of FG-CNTRCs cylindrical circular shells based on TSDT considering the material properties as temperature-dependent and also be rested on a viscoelastic foundation. The CNTs distribution is assumed to be FG in the thickness of the shell and the extended rule of mixture (ERM) is used to determine the effective values of different properties of the shell. The structure is subjected to the electro-magnetic fields and loads. The governing equations of motion will be obtained using Hamilton's principle and variational formulation and will be solved analytically via Navier's method to obtain the results. The results for simpler states will be verified with the previous studies and the effect of different parameters on the results will be discussed in details.

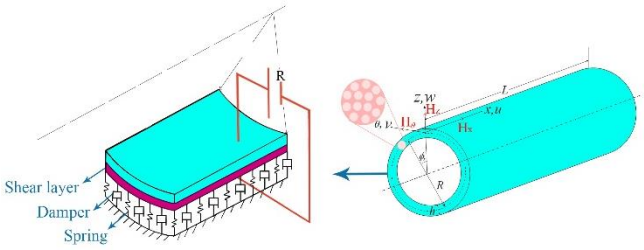

Fig. 1 Schematic of the MEE FG-CNTRC cylindrical circular shell subjected to electro-magnetic fields and resting on visco-Winkler-Pasternak elastic foundation

2. Theoretical formulation

An MEE FG-CNTRC thick cylindrical shell which is resting on visco-Pasternak elastic foundation and its properties change with temperature variations is under consideration and is shown in Fig. 1. Radius, length, thickness and rotation angle of the shell respectively are presented by R, L, h and ϕ_r. It also supposed that the CNTs are used as the reinforcement of the nano-composite with PVDF matrix and are placed in longitudinal direction.

The displacement components of the shell are described using cylindrical coordinate system (x, θ, z) which the axial and circumferential directions are respectively shown by x and θ and also z is in normal to the mid-surface direction. The corner of the shell in the middle plane is selected to locate the origin of the coordinate system.

2.1 Material properties

The effective properties of the considering shell can be achieved using ERM. According to ERM, the properties of the shell i.e. Young's and shear moduli can be obtained using the following relations (Amir *et al*. 2017, Ghorbanpour Arani *et al*. 2018a):

$$E_{11} = \eta_1 V_{CNT} E_{11}^{CNT} + V_m E_m \tag{1}$$

$$\frac{\eta_2}{E_{22}} = \frac{V_{CNT}}{E_{22}^{CNT}} + \frac{V_m}{E_m} \tag{2}$$

$$\frac{\eta_3}{G_{12}} = \frac{V_{CNT}}{G_{12}^{CNT}} + \frac{V_m}{G_m} \tag{3}$$

in which E_{11}^{CNT}, E_{22}^{CNT}, G_{12}^{CNT}, E_m and G_m are longitudinal and transversely Young's and shear moduli of the CNTs and matrix, respectively. Also, V_{CNT} is CNTs volume fraction which depends on CNTs distribution pattern and V_m represents volume fraction of matrix and $V_{CNT} + V_m = 1$. It should be noted that PVDF is considered as matrix in this paper. η_1, η_2, and η_3 are efficiency parameters of CNTs which are determined by molecular dynamics simulation.

Also the mixture rule can be developed for other properties of the CNTRC shell i.e. magnetic and electric ones as follows (Ghorbanpour Arani *et al*. 2012):

$$P_{ij} = V_{CNT} P_{ij}^{CNT} + V_m P_{ij}^{m} \tag{4}$$

where P_{ij} represents the effective properties of the shell and P_{ij}^{CNT} and P_{ij}^{m} demonstrate the same property for the CNTs and matrix, respectively. P_{ij} indicates different mechanical and electro-magnetic properties of the shell such as density, piezoelectric and magnetic coefficients, electro-magnetic coupling and dielectric and magnetic permeability. However, the Poisson's ratio varies through the following relation (Mohammadimehr *et al*. 2016c):

$$\nu_{12} = V_{CNT}^{*} \nu_{12}^{CNT} + V_m \nu_m \tag{5}$$

Also, the CNTs volume fraction is presented by V_{CNT}^{*} and defined as:

$$V_{CNT}^{*} = \frac{w_{CNT}}{w_{CNT} + \left(\frac{\rho_{CNT}}{\rho_m}\right) - \left(\frac{\rho_{CNT}}{\rho_m}\right) w_{CNT}} \tag{6}$$

in which w_{CNT} denotes the mass density of the CNTs and ρ_{CNT} and ρ_m are densities of the CNTs and matrix, respectively.

The CNTs are distributed FG in the thickness direction of the cylindrical shell as five different following patterns (Mohammadimehr *et al*. 2018c):

$$V_{CNT} = V_{CNT}^{*} \quad (\text{for } \textit{Uniform} \text{ distribution}) \tag{7}$$

$$V_{CNT} = \left(1 + \frac{2z}{h}\right) V_{CNT}^{*} \quad (\text{for } FG-V \text{ distribution}) \tag{8}$$

$$V_{CNT} = \left(1 - \frac{2|z|}{h}\right) V_{CNT}^{*} \quad (\text{for } FG-A \text{ distribution}) \tag{9}$$

$$V_{CNT} = 2\left(\frac{2|z|}{h}\right) V_{CNT}^{*} \quad (\text{for } FG-X \text{ distribution}) \tag{10}$$

$$V_{CNT} = 2\left(1 - \frac{2|z|}{h}\right) V_{CNT}^{*} \quad (\text{for } FG-X \text{ distribution}) \tag{11}$$

Fig. 2 shows the mentioned patterns respect to the thickness of the shell.

Furthermore, the properties of the CNTs reinforcement and PVDF are considered as temperature-dependent. The following polynomial function is estimated for dependence to temperature for CNTs (Jooybar *et al*. 2016):

$$P_{CNTf}(T) = P_0 (1 + P_1 \Delta T + P_2 \Delta T^2 + P_3 \Delta T^3) \tag{12}$$

P_0, P_1, P_2, and P_3 are temperature-dependent properties coefficients of CNTs and ΔT indicates temperature change from the room temperature.

Temperature-dependent properties of PVDF can be obtained using experimental methods (Laiarinandrasana *et al*. 2009). The following function is estimated to this purpose as follows:

$$\begin{aligned} P_{mf}(T) = & -(1.1905)T^5 + (1.5783\times10^3)T^4 \\ & -(8.3608\times10^5)T^3 + (2.2122\times10^8)T^2 \\ & -(2.9257\times10^{10})T + (1.5519\times10^{12}) \end{aligned} \tag{13}$$

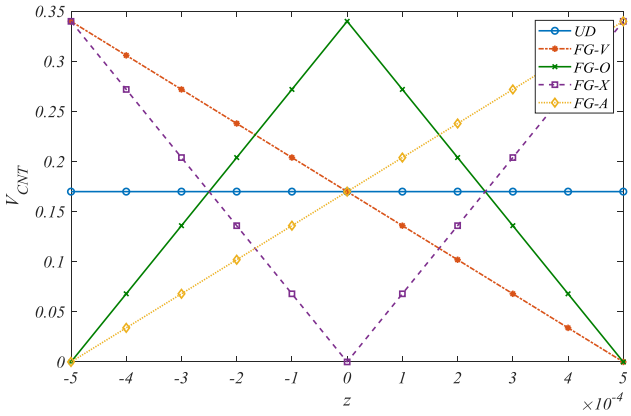

Fig. 2 Various patterns of CNTs distribution along the thickness of the FG-CNTRC shell. (V^*_{CNT} =0.17)

where T is the temperature in Kelvin.

2.2 Displacement field

Since the considering shell is thick, the TSDT or Reddy's theory is employed to describe the displacement components as follows (Reddy 2004):

$$\begin{aligned} u_x(x,\theta,z,t) &= u(x,\theta,t)+z\varphi_1(x,\theta,t) \\ &\quad +z^2\lambda_1(x,\theta,t)+z^3\beta_1(x,\theta,t) \\ u_\theta(x,\theta,z,t) &= v(x,\theta,t)+z\varphi_2(x,\theta,t) \\ &\quad +z^2\lambda_2(x,\theta,t)+z^3\beta_2(x,\theta,t) \\ u_z(x,\theta,z,t) &= w(x,\theta,t) \end{aligned} \tag{14}$$

By satisfying the stress-free condition in the surfaces of the shell which is equivalent to $\tau_{xz}=\tau_{\theta z}=0$ at $z=\pm h/2$, Eq. (14) can be simplified in the following form (Yahiaoui *et al*. 2018):

$$\begin{aligned} u_x(x,\theta,z,t) &= u(x,\theta,t)+z\varphi_1(x,\theta,t) \\ &\quad -c_1z^3\left(\varphi_1(x,\theta,t)+\frac{\partial w(x,\theta,t)}{\partial x}\right) \\ u_\theta(x,\theta,z,t) &= v(x,\theta,t)+z\varphi_2(x,\theta,t) \\ &\quad -c_1z^3\left(\varphi_2(x,\theta,t)+\frac{1}{R}\frac{\partial w(x,\theta,t)}{\partial \theta}\right) \\ u_z(x,\theta,z,t) &= w(x,\theta,t) \end{aligned} \tag{15}$$

in which u_x, u_θ and u_z are the displacements of an arbitrary point of the shell in x, θ and z directions, respectively and u, v and w represent the middle plane of the shell displacement components in x, θ and z directions, respectively. Also, φ_1 and φ_2 are the rotation of the middle plane about θ and x axes and $c_1=4/3h^2$, respectively.

The strain-displacement relations based on the TSDT displacement field can be written as:

$$\varepsilon_{xx}=\varepsilon^{(0)}_{xx}+zk^{(1)}_{xx}+c_1z^3k^{(3)}_{xx} \tag{16}$$

$$\varepsilon_{\theta\theta}=\varepsilon^{(0)}_{\theta\theta}+zk^{(1)}_{\theta\theta}+c_1z^3k^{(3)}_{\theta\theta}$$

$$\gamma_{x\theta}=\gamma^{(0)}_{x\theta}+zk^{(1)}_{x\theta}+c_1z^3k^{(3)}_{x\theta}$$

$$\gamma_{xz}=\gamma^{(0)}_{xz}+3c_1z^2k^{(2)}_{xz}$$

$$\gamma_{\theta z}=\gamma^{(0)}_{\theta z}-3c_1z^2k^{(2)}_{\theta z}$$

where $\varepsilon^{(0)}_{xx}$, $\varepsilon^{(0)}_{\theta\theta}$, $\gamma^{(0)}_{x\theta}$, $\gamma^{(0)}_{xz}$ and $\gamma^{(0)}_{\theta z}$ are the middle plane strain components and $k^{(k)}_{ij}$ (i, j=x, θ, z and k=1, 2, 3) are the curvatures and are given in "Appendix A".

2.3 Stress-strain relations

The constitutive relations for an MEE FG-CNTRC cylindrical shell are defined as follow (Mohammadimehr *et al*. 2018a):

$$\begin{Bmatrix}\sigma_{xx}\\ \sigma_{\theta\theta}\\ \tau_{\theta z}\\ \tau_{xz}\\ \tau_{x\theta}\end{Bmatrix}=\begin{bmatrix}Q_{11}&Q_{12}&0&0&0\\ Q_{12}&Q_{22}&0&0&0\\ 0&0&Q_{44}&0&0\\ 0&0&0&Q_{55}&0\\ 0&0&0&0&Q_{66}\end{bmatrix}\begin{Bmatrix}\varepsilon_{xx}\\ \varepsilon_{\theta\theta}\\ \gamma_{\theta z}\\ \gamma_{xz}\\ \gamma_{x\theta}\end{Bmatrix} -\begin{bmatrix}0&0&e_{31}\\ 0&0&e_{32}\\ 0&e_{24}&0\\ e_{15}&0&0\\ 0&0&0\end{bmatrix}\begin{Bmatrix}E_x\\ E_\theta\\ E_z\end{Bmatrix}-\begin{bmatrix}0&0&q_{31}\\ 0&0&q_{32}\\ 0&q_{24}&0\\ q_{15}&0&0\\ 0&0&0\end{bmatrix}\begin{Bmatrix}H_x\\ H_\theta\\ H_z\end{Bmatrix} \tag{17}$$

where e_{ij} piezo-electric coefficients, q_{ij} piezo-magnetic coefficients, E_i, and H_i are electric and magnetic fields components, respectively and Q_{ij} are stiffness matrix components and are defined as follow (Mohammadimehr *et al*. 2018b):

$$\begin{aligned} Q_{11}&=\frac{E_{11}}{1-\nu_{12}\nu_{21}}, & Q_{12}&=\nu_{21}Q_{11}, \\ Q_{22}&=\frac{E_{22}}{1-\nu_{12}\nu_{21}}, & Q_{44}&=G_{23}, \\ Q_{55}&=G_{13}, & Q_{66}&=G_{12} \end{aligned} \tag{18}$$

Also, the electric and magnetic displacements can be introduced using the following relations (Shooshtari and Razavi 2016):

$$\begin{Bmatrix}D_x\\ D_\theta\\ D_z\end{Bmatrix}=\begin{bmatrix}0&0&0&e_{15}&0\\ 0&0&e_{24}&0&0\\ e_{31}&e_{32}&0&0&0\end{bmatrix}\begin{Bmatrix}\varepsilon_{xx}\\ \varepsilon_{\theta\theta}\\ \gamma_{\theta z}\\ \gamma_{xz}\\ \gamma_{x\theta}\end{Bmatrix} +\begin{bmatrix}s_{11}&0&0\\ 0&s_{22}&0\\ 0&0&s_{33}\end{bmatrix}\begin{Bmatrix}E_x\\ E_\theta\\ E_z\end{Bmatrix}+\begin{bmatrix}d_{11}&0&0\\ 0&d_{22}&0\\ 0&0&d_{33}\end{bmatrix}\begin{Bmatrix}H_x\\ H_\theta\\ H_z\end{Bmatrix} \tag{19}$$

$$\begin{Bmatrix} B_x \\ B_\theta \\ B_z \end{Bmatrix} = \begin{bmatrix} 0 & 0 & 0 & q_{15} & 0 \\ 0 & 0 & q_{24} & 0 & 0 \\ q_{31} & q_{32} & 0 & 0 & 0 \end{bmatrix} \begin{Bmatrix} \varepsilon_{xx} \\ \varepsilon_{\theta\theta} \\ \gamma_{\theta z} \\ \gamma_{xz} \\ \gamma_{x\theta} \end{Bmatrix} + \begin{bmatrix} d_{11} & 0 & 0 \\ 0 & d_{22} & 0 \\ 0 & 0 & d_{33} \end{bmatrix} \begin{Bmatrix} E_x \\ E_\theta \\ E_z \end{Bmatrix} + \begin{bmatrix} \mu_{11} & 0 & 0 \\ 0 & \mu_{22} & 0 \\ 0 & 0 & \mu_{33} \end{bmatrix} \begin{Bmatrix} H_x \\ H_\theta \\ H_z \end{Bmatrix} \tag{20}$$

where s_{ii}, $d_{ii,}$ and μ_{ii} are dielectric permeability, magneto-electric coefficients and magnetic permeability, respectively and D_i and B_i represent electric and magnetic displacements, respectively.

The electric and magnetic fields should be selected in such a way to satisfy Maxwell's relation. So they can be expressed as follows (Arshid *et al*. 2019):

$$E = -\nabla\Phi, \tag{21}$$

$$H = -\nabla\Psi \tag{22}$$

The electric and magnetic potentials are distributed through the thickness as follows (Arefi *et al*. 2018):

$$\Phi(x,\theta,z,t) = \frac{2z}{h}V_E - \phi(x,\theta,t)\cos\left(\frac{\pi z}{h}\right), \tag{23}$$

$$\Psi(x,\theta,z,t) = \frac{2z}{h}\Omega - \psi(x,\theta,t)\cos\left(\frac{\pi z}{h}\right) \tag{24}$$

where V_E and Ω are the external applied electric and magnetic potential, respectively. Accordingly, the electric and magnetic fields components in three directions are as:

$$\begin{aligned} &\{E_x, E_\theta\} = -\left\{\frac{\partial\Phi}{\partial x}, \frac{1}{R}\frac{\partial\Phi}{\partial\theta}\right\} = \left\{\frac{\partial\phi}{\partial x}, \frac{1}{R}\frac{\partial\phi}{\partial\theta}\right\}\cos\left(\frac{\pi z}{h}\right), \\ &E_z = -\frac{\partial\Phi}{\partial z} = -\frac{2}{h}V_E - \frac{\pi}{h}\phi\sin\left(\frac{\pi z}{h}\right) \end{aligned} \tag{25}$$

$$\begin{aligned} &\{H_x, H_\theta\} = -\left\{\frac{\partial\Psi}{\partial x}, \frac{1}{R}\frac{\partial\Psi}{\partial\theta}\right\} = \left\{\frac{\partial\psi}{\partial x}, \frac{1}{R}\frac{\partial\psi}{\partial\theta}\right\}\cos\left(\frac{\pi z}{h}\right), \\ &\mathrm{H}_z = -\frac{\partial\Psi}{\partial z} = -\frac{2}{h}\Omega - \frac{\pi}{h}\psi\sin\left(\frac{\pi z}{h}\right) \end{aligned} \tag{26}$$

3. Governing equations

3.1 Hamilton's principle

Hamilton's principle is used to extract the motion equations. This principle expresses that the difference of strain energy and the sum of kinetic energy and external work variations in a specific period should be equal to zero as follow (Arshid and Khorshidvand 2018, Bennoun *et al*. 2016, El-Haina *et al*. 2017):

$$\int_{t_1}^{t_2} (\delta U - \delta K - \delta W)\mathrm{d}t = 0 \tag{27}$$

Here strain and kinetic energies respectively are shown by U and K. Also W indicates the external work.

3.2 Strain energy

Following relation can be employed to obtain the strain energy of the shell (Amir *et al*. 2018):

$$U = \frac{1}{2}\iiint_{x\,\theta\,z} (\sigma_{ij}\varepsilon_{ij} - D_i E_i - B_i H_i) R\mathrm{d}x\mathrm{d}\theta\mathrm{d}z \tag{28}$$

Using variational formulation, Eq. (28) is written in the following form:

$$\delta U = \int_{-h/2}^{h/2}\iint_{x\,\theta} \begin{pmatrix} \sigma_{xx}\delta\varepsilon_{xx} + \sigma_{\theta\theta}\delta\varepsilon_{\theta\theta} + \tau_{x\theta}\delta\gamma_{x\theta} \\ +\tau_{xz}\delta\gamma_{xz} + \tau_{\theta z}\delta\gamma_{\theta z} \\ -D_x\delta E_x - D_\theta\delta E_\theta - D_z\delta E_z \\ -B_x\delta H_x - B_\theta\delta H_\theta - B_z\delta H_z \end{pmatrix} R dx d\theta dz \tag{29}$$

Substituting stress-strain relations using Eq.s (17), (19) and (20) in Eq. (28), yields:

$$\delta U = \iint_{x\,\theta} \begin{pmatrix} RN_{xx}\dfrac{\partial\delta u}{\partial x} + RP_\theta\delta\varphi_2 + \bar{B}_\theta\dfrac{\partial\delta\psi}{\partial\theta} \\ +\bar{D}_\theta\dfrac{\partial\delta\phi}{\partial\theta} + RP_x\dfrac{\partial\delta w}{\partial x} + RN_{x\theta}\dfrac{\partial\delta v}{\partial x} \\ +RP_x\delta\varphi_1 - Q_\theta\delta\varphi_2 + M_{\theta\theta}\dfrac{\partial\delta\varphi_2}{\partial\theta} \\ +M_{x\theta}\dfrac{\partial\delta\varphi_1}{\partial\theta} - 3RR_x c_1\delta\varphi_1 - 3RR_x c_1\dfrac{\partial\delta w}{\partial x} \\ -RH_{xx}c_1\dfrac{\partial\delta\varphi_1}{\partial x} - RH_{xx}c_1\dfrac{\partial^2\delta w}{\partial x^2} - 3RR_\theta c_1\delta\varphi_2 \\ -RH_{x\theta}c_1\dfrac{\partial\delta\varphi_2}{\partial x} - \dfrac{H_{\theta\theta}c_1}{R}\dfrac{\partial^2\delta w}{\partial\theta^2} \\ +\dfrac{V_\theta c_1}{R}\dfrac{\partial\delta w}{\partial\theta} - R\bar{B}_z\delta\psi - R\bar{D}_z\delta\phi \\ +P_\theta\dfrac{\partial\delta w}{\partial\theta} - P_\theta\delta v + N_{x\theta}\dfrac{\partial\delta u}{\partial\theta} + N_{\theta\theta}\dfrac{\partial\delta v}{\partial\theta} \\ +N_{\theta\theta}\delta w - R_\theta c_1\dfrac{\partial\delta w}{\partial\theta} + V_\theta c_1\delta\varphi_2 - H_{x\theta}c_1\dfrac{\partial\delta\varphi_1}{\partial\theta} \\ -2H_{x\theta}c_1\dfrac{\partial^2\delta w}{\partial x\partial\theta} + RM_{x\theta}\dfrac{\partial\delta\varphi_2}{\partial x} + R\bar{D}_x\dfrac{\partial\delta\phi}{\partial x} \\ +RM_{xx}\dfrac{\partial\delta\varphi_1}{\partial x} + R\bar{B}_x\dfrac{\partial\delta\psi}{\partial x} - H_{\theta\theta}c_1\dfrac{\partial\delta\varphi_2}{\partial\theta} \end{pmatrix} \mathrm{d}x\,\mathrm{d}\theta \tag{30}$$

The mentioned coefficients in Eq. (30) are defined as:

$$\{N_{ij},\ M_{ij},\ H_{ij}\} = \int_{-h/2}^{h/2} \{1,\ z,\ z^3\}\sigma_{ij}\,\mathrm{d}z, \quad i,j = x,\theta \tag{31}$$

$$\{P_i,\ R_i\} = \int_{-h/2}^{h/2} \{1,\ z^2\}\tau_{iz}\,\mathrm{d}z, \qquad i = x,\theta \tag{32}$$

$$\bar{B}_j = \int_{-h/2}^{h/2} B_j\cos\left(\frac{\pi z}{h}\right)\mathrm{d}z, \qquad j = x,\theta \tag{33}$$

$$\bar{B}_z = \int_{-h/2}^{h/2} \left[\frac{\pi}{h}\right] B_z\sin\left(\frac{\pi z}{h}\right)\mathrm{d}z, \tag{34}$$

$$\bar{D}_j = \int_{-h/2}^{h/2} D_j\cos\left(\frac{\pi z}{h}\right)\mathrm{d}z, \qquad j = x,\theta \tag{35}$$

$$\bar{D}_z = \int_{-h/2}^{h/2} \left[\frac{\pi}{h}\right] D_z \sin\left(\frac{\pi z}{h}\right) \mathrm{d}z \tag{36}$$

3.3 Kinetic energy

The kinetic energy of the MEE FG-CNTRC shell can be determined using the following relation (Arshid & Khorshidvand 2017, Belmahi *et al*. 2018):

$$K = \frac{1}{2}\iiint_{x\,\theta\,z} \rho(z)\left(\left(\frac{\partial u_x}{\partial t}\right)^2 + \left(\frac{\partial u_\theta}{\partial t}\right)^2 + \left(\frac{\partial u_z}{\partial t}\right)^2\right) R\mathrm{d}x\mathrm{d}\theta\mathrm{d}z \tag{37}$$

The variations of the kinetic energy in a specific period is as follow:

$$\int_{t_1}^{t_2} \delta K \,\mathrm{d}t = \int_{t_1}^{t_2}\int_{-h/2}^{h/2}\iint_{x\,\theta} \rho(z)\begin{pmatrix} \frac{\partial u_x}{\partial t}\frac{\partial \delta u_x}{\partial t} + \frac{\partial u_\theta}{\partial t}\frac{\partial \delta u_\theta}{\partial t} \\ + \frac{\partial u_z}{\partial t}\frac{\partial \delta u_z}{\partial t} \end{pmatrix} R\,\mathrm{d}x\,\mathrm{d}\theta\,\mathrm{d}z\,\mathrm{d}t; \tag{38}$$

Substituting displacements from Eq. (15) into Eq. (38), the following relation for the kinetic energy variations can be obtained:

$$\int_{t_1}^{t_2} \delta K \,\mathrm{d}t = \int_{t_1}^{t_2}\int_{-h/2}^{h/2}\iint_{x\,\theta} \rho(z)\begin{pmatrix} \left(\frac{\partial u}{\partial t} + z\frac{\partial \varphi_1}{\partial t} - c_1 z^3\left(\frac{\partial \varphi_1}{\partial t} + \frac{\partial^2 w}{\partial t\partial x}\right)\right) \\ \left(\frac{\partial \delta u}{\partial t} + z\frac{\partial \delta\varphi_1}{\partial t} - c_1 z^3\left(\frac{\partial \delta\varphi_1}{\partial t} + \frac{\partial^2 \delta w}{\partial t\partial x}\right)\right) \\ +\left(\frac{\partial v}{\partial t} + z\frac{\partial \varphi_2}{\partial t} - c_1 z^3\left(\frac{\partial}{\partial t}\varphi_2 + \frac{1}{R}\frac{\partial^2 w}{\partial t\partial\theta}\right)\right) \\ \left(\frac{\partial \delta v}{\partial t} + z\frac{\partial \delta\varphi_2}{\partial t} - c_1 z^3\left(\frac{\partial \delta\varphi_2}{\partial t} + \frac{1}{R}\frac{\partial^2 \delta w}{\partial t\partial\theta}\right)\right) \\ +\left(\frac{\partial w}{\partial t}\right)\left(\frac{\partial \delta w}{\partial t}\right) \end{pmatrix} R\,\mathrm{d}x\,\mathrm{d}\theta\,\mathrm{d}z\,\mathrm{d}t \tag{39}$$

Accordingly:

$$\int_{t_1}^{t_2} \delta K \,\mathrm{d}t = \int_{t_1}^{t_2}\iint_{x\,\theta} \begin{pmatrix} I_0\frac{\partial u}{\partial t}\frac{\partial \delta u}{\partial t} + I_1\frac{\partial u}{\partial t}\frac{\partial \delta\varphi_1}{\partial t} - c_1 I_3\frac{\partial u}{\partial t}\frac{\partial \delta\varphi_1}{\partial t} \\ -c_1 I_3\frac{\partial u}{\partial t}\frac{\partial^2 \delta w}{\partial t\partial x} + I_1\frac{\partial \varphi_1}{\partial t}\frac{\partial \delta u}{\partial t} + I_2\frac{\partial \varphi_1}{\partial t}\frac{\partial \delta\varphi_1}{\partial t} \\ -c_1 I_4\frac{\partial \varphi_1}{\partial t}\frac{\partial \delta\varphi_1}{\partial t} - c_1 I_4\frac{\partial \varphi_1}{\partial t}\frac{\partial^2 \delta w}{\partial t\partial x} - c_1 I_3\frac{\partial \varphi_1}{\partial t}\frac{\partial \delta u}{\partial t} \\ -c_1 I_4\frac{\partial \varphi_1}{\partial t}\frac{\partial \delta\varphi_1}{\partial t} + c_1^2 I_6\frac{\partial \varphi_1}{\partial t}\frac{\partial \delta\varphi_1}{\partial t} + c_1^2 I_6\frac{\partial \varphi_1}{\partial t}\frac{\partial^2 \delta w}{\partial t\partial x} \\ -c_1 I_3\frac{\partial^2 w}{\partial t\partial x}\frac{\partial \delta u}{\partial t} - c_1 I_4\frac{\partial^2 w}{\partial t\partial x}\frac{\partial \delta\varphi_1}{\partial t} + c_1^2 I_6\frac{\partial^2 w}{\partial t\partial x}\frac{\partial \delta\varphi_1}{\partial t} \\ +c_1^2 I_6\frac{\partial^2 w}{\partial t\partial x}\frac{\partial^2 \delta w}{\partial t\partial x} + I_0\frac{\partial v}{\partial t}\frac{\partial \delta v}{\partial t} + I_1\frac{\partial v}{\partial t}\frac{\partial \delta\varphi_2}{\partial t} \\ -c_1 I_3\frac{\partial v}{\partial t}\frac{\partial \delta\varphi_2}{\partial t} - c_1 I_3\frac{1}{R}\frac{\partial v}{\partial t}\frac{\partial^2 \delta w}{\partial t\partial\theta} + I_1\frac{\partial \varphi_2}{\partial t}\frac{\partial \delta v}{\partial t} \\ +I_2\frac{\partial \varphi_2}{\partial t}\frac{\partial \delta\varphi_2}{\partial t} - Rc_1 I_4\frac{1}{R}\frac{\partial \varphi_2}{\partial t}\frac{\partial \delta\varphi_2}{\partial t} - c_1 I_4\frac{1}{R}\frac{\partial \varphi_2}{\partial t}\frac{\partial^2 \delta w}{\partial t\partial\theta} \\ -c_1 I_3\frac{\partial \varphi_2}{\partial t}\frac{\partial \delta v}{\partial t} - c_1 I_4\frac{\partial \varphi_2}{\partial t}\frac{\partial \delta\varphi_2}{\partial t} + c_1^2 I_6\frac{\partial \varphi_2}{\partial t}\frac{\partial \delta\varphi_2}{\partial t} \\ +c_1^2 I_6\frac{1}{R}\frac{\partial \varphi_2}{\partial t}\frac{\partial^2 \delta w}{\partial t\partial\theta} - c_1 I_3\frac{1}{R}\frac{\partial^2 w}{\partial t\partial\theta}\frac{\partial \delta v}{\partial t} - c_1 I_4\frac{1}{R}\frac{\partial^2 w}{\partial t\partial\theta}\frac{\partial \delta\varphi_2}{\partial t} \\ +c_1^2 I_6\frac{1}{R}\frac{\partial^2 w}{\partial t\partial\theta}\frac{\partial \delta\varphi_2}{\partial t} + c_1^2 I_6\frac{1}{R^2}\frac{\partial^2 w}{\partial t\partial\theta}\frac{\partial^2 \delta w}{\partial t\partial\theta} + I_0\frac{\partial w}{\partial t}\frac{\partial \delta w}{\partial t} \end{pmatrix} R\,\mathrm{d}x\,\mathrm{d}\theta\,\mathrm{d}t; \tag{40}$$

in which:

$$I_k = \int_z \rho(z)\, z^k \,\mathrm{d}z, \qquad k = 0,1,...,6 \tag{41}$$

3.4 External work

In the present research the total work is the sum of electro-magnetic potentials and viscoelastic foundation force (Ozdemir 2018):

$$W = W_{ext} + W_{found} \tag{42}$$

in which W_{ext} and W_{found} respectively indicate the work of electro-magnetic loads and viscoelastic foundation force.

The following expression can be used to obtain the work of electro-magnetic loads (Ghorbanpour Arani *et al*. 2017b, Mohammadimehr *et al*. 2017b):

$$W_{ext} = \frac{1}{2}\int_x\int_\theta \left\{N_x^{ext}\left(\frac{\partial w}{\partial x}\right)^2 + \frac{1}{R^2}N_\theta^{ext}\left(\frac{\partial w}{\partial \theta}\right)^2\right\} R\,\mathrm{d}x\,\mathrm{d}\theta \tag{43}$$

where N_x^{ext} and N_θ^{ext} are the external loads in the axial and circumferential directions and consist of electro-magnetic loads as follows:

$$N_x^{ext} = N_x^E + N_x^H, \tag{44}$$

$$N_\theta^{ext} = N_\theta^E + N_\theta^H \tag{45}$$

Here, N_i^E and N_i^H (i= x, θ) are the electro-magnetic loads and are defined as:

$$\begin{Bmatrix} N_x^E & N_\theta^E \end{Bmatrix} = -2\begin{Bmatrix} e_{31} & e_{32} \end{Bmatrix} V_E, \tag{46}$$

$$\begin{Bmatrix} N_x^H & N_\theta^H \end{Bmatrix} = -2\begin{Bmatrix} q_{31} & q_{32} \end{Bmatrix} \Omega \tag{47}$$

Also, the variations of work done by the visco-Pasternak elastic foundation which the shell is resting on it can be written as (Duc & Quan 2015, Meksi *et al*. 2015):

$$\delta W_{found} = \iint_A F_{found}\, \delta w \,\mathrm{d}A; \tag{48}$$

in which the foundation force consists of three parts: the spring force, the shear layer force and the damping force (Amir 2016, Ghorbanpour Arani *et al*. 2018b):

$$F_{found} = K_W w - K_G \nabla^2 w + C_d \frac{\partial w}{\partial t} \tag{49}$$

It is noticeable that K_W, K_G, and C_d represent Winkler, Pasternak and damping constants, respectively and Laplacian operator is shown by ∇^2.

3.5 Governing motion equations

The motion equations are achieved based on Eqs. (30), (40), (42) and Hamilton's principle as follows:

δu:

$$\frac{\partial N_{xx}}{\partial x} + \frac{1}{R}\frac{\partial N_{x\theta}}{\partial \theta} = I_0\frac{\partial^2 u}{\partial t^2} + I_1\frac{\partial^2 \varphi_1}{\partial t^2} - I_3 c_1\left(\frac{\partial^2 \varphi_1}{\partial t^2} + \frac{\partial^3 w}{\partial x \partial t^2}\right) \tag{50}$$

δv:

$$\frac{\partial N_{x\theta}}{\partial x} + \frac{1}{R}\frac{\partial N_{\theta\theta}}{\partial \theta} = I_0\frac{\partial^2 v}{\partial t^2} + I_1\frac{\partial^2 \varphi_2}{\partial t^2} - I_3 c_1\left(\frac{\partial^2 \varphi_2}{\partial t^2} + \frac{1}{R}\frac{\partial^3 w}{\partial \theta \partial t^2}\right) \tag{51}$$

δw:

$$\begin{aligned}&-3c_1\frac{\partial R_x}{\partial x}+c_1\frac{\partial^2 H_{xx}}{\partial x^2}+\frac{c_1}{R^2}\frac{\partial^2 H_{\theta\theta}}{\partial\theta^2}+\frac{2}{R}c_1\frac{\partial^2 H_{x\theta}}{\partial x\partial\theta}-\frac{3}{R}c_1\frac{\partial R_\theta}{\partial\theta}+\frac{\partial P_x}{\partial x}\\&-\frac{1}{R}N_{\theta\theta}+\frac{1}{R}\frac{\partial P_\theta}{\partial\theta}-K_W w+K_G\nabla^2 w-C_d\frac{\partial w}{\partial t}-N_x^{ext}\frac{\partial^2 w}{\partial x^2}-\frac{1}{R^2}N_\theta^{ext}\frac{\partial^2 w}{\partial\theta^2}\\&=I_0\frac{\partial^2 w}{\partial t^2}+I_3c_1\left(\frac{\partial^3 u}{\partial x\partial t^2}+\frac{1}{R}\frac{\partial^3 v}{\partial\theta\partial t^2}\right)+I_4c_1\left(\frac{\partial^3\varphi_1}{\partial x\partial t^2}+\frac{1}{R}\frac{\partial^3\varphi_2}{\partial\theta\partial t^2}\right)\\&-I_6c_1^2\left(\frac{\partial^3\varphi_1}{\partial x\partial t^2}+\frac{\partial^4 w}{\partial x^2\partial t^2}+\frac{1}{R}\frac{\partial^3\varphi_2}{\partial\theta\partial t^2}+\frac{1}{R^2}\frac{\partial^4 w}{\partial\theta^2\partial t^2}\right)\end{aligned}\tag{52}$$

$\delta\varphi_1$:

$$\begin{aligned}&3c_1R_x-\frac{1}{R}c_1\frac{\partial H_{x\theta}}{\partial\theta}-c_1\frac{\partial H_{xx}}{\partial x}-P_x+\frac{\partial M_{xx}}{\partial x}+\frac{1}{R}\frac{\partial M_{x\theta}}{\partial\theta}=I_1\frac{\partial^2 u}{\partial t^2}+I_2\frac{\partial^2\varphi_1}{\partial t^2}-I_3c_1\frac{\partial^2 u}{\partial t^2}\\&-I_4c_1\left(2\frac{\partial^2\varphi_1}{\partial t^2}+\frac{\partial^3 w}{\partial x\partial t^2}\right)+I_6c_1^2\left(\frac{\partial^2\varphi_1}{\partial t^2}+\frac{\partial^3 w}{\partial x\partial t^2}\right)\end{aligned}\tag{53}$$

$\delta\varphi_2$:

$$\begin{aligned}&3c_1R_\theta-\frac{1}{R}c_1\frac{\partial H_{\theta\theta}}{\partial\theta}-c_1\frac{\partial H_{x\theta}}{\partial x}-P_\theta+\frac{\partial M_{x\theta}}{\partial x}+\frac{1}{R}\frac{\partial M_{\theta\theta}}{\partial\theta}=I_1\frac{\partial^2 v}{\partial t^2}+I_2\frac{\partial^2\varphi_2}{\partial t^2}\\&-I_3c_1\frac{\partial^2 v}{\partial t^2}-I_4c_1\left(2\frac{\partial^2\varphi_2}{\partial t^2}+\frac{1}{R}\frac{\partial^3 w}{\partial\theta\partial t^2}\right)+I_6c_1^2\left(\frac{\partial^2\varphi_2}{\partial t^2}+\frac{1}{R}\frac{\partial^3 w}{\partial\theta\partial t^2}\right)\end{aligned}\tag{54}$$

$\delta\phi$:

$$\frac{\partial\bar{D}_x}{\partial x}+\frac{1}{R}\frac{\partial\bar{D}_\theta}{\partial\theta}+\bar{D}_z=0\tag{55}$$

$\delta\psi$:

$$\frac{\partial\bar{B}_x}{\partial x}+\frac{1}{R}\frac{\partial\bar{B}_\theta}{\partial\theta}+\bar{B}_z=0\tag{56}$$

4. Navier's method

According to Navier's method, the displacement components are defined such a way to satisfy the boundary condition for the simply supported ends cylindrical shell. Therefore, the displacement variables can be expressed as follows (Zaoui *et al*. 2019):

$$\begin{Bmatrix}u\\v\\w\\\varphi_1\\\varphi_2\\\phi\\\psi\end{Bmatrix}=\sum_{m=1}^{\infty}\sum_{n=1}^{\infty}\begin{Bmatrix}\bar{u}\sin(\beta_m\theta)\cos(P_nx)\\\bar{v}\cos(\beta_m\theta)\sin(P_nx)\\\bar{w}\sin(\beta_m\theta)\sin(P_nx)\\\bar{\varphi}_1\sin(\beta_m\theta)\cos(P_nx)\\\bar{\varphi}_2\cos(\beta_m\theta)\sin(P_nx)\\\bar{\phi}\sin(\beta_m\theta)\sin(P_nx)\\\bar{\psi}\sin(\beta_m\theta)\sin(P_nx)\end{Bmatrix}e^{i\omega t}\tag{57}$$

where

$$\beta_m=\frac{m\pi}{\phi_r},\qquad P_n=\frac{n\pi}{L}\tag{58}$$

Maximum values of displacements, electric and magnetic potentials which are unknown respectively are shown by $\bar{u}$, $\bar{v}$, $\bar{w}$, $\bar{\varphi}_1$, $\bar{\varphi}_2$, $\bar{\phi}$ and $\bar{\psi}$. Should be noted that m and n are the axial and circumferential wave numbers, respectively, and ω represents the natural frequency. Substituting the functions of Eq. (57) in the Eq.s (50)-(56), yields:

$$\left([K]+i\omega[C]-\omega^2[M]\right)\{d\}=\{0\}\tag{59}$$

Table 1 Temperature-independent material properties of SWCNTs (Mohammadimehr *et al*. 2018a)

Properties	Value
v	0.175
ρ (kg/m^3)	1400
e_{31} (C/m^2)	0
q_{31} (N/Am)	22
d_{33} (Ns/CV)	0
μ_{33} (Ns^2/C^2)	0.25
s_{33} (C/Vm)	0

Table 2 Efficiency parameters of CNTs (Mohammadimehr *et al*. 2018a)

V_{CNT}^*	η_1	η_2	η_3
0.12	0.137	1.022	0.715
0.17	0.142	1.626	1.138
0.28	0.141	1.585	1.109

Table 3 Temperature-independent material properties of PVDF (Mohammadimehr *et al*. 2018b)

Properties	Value
ρ (kg/m^3)	1780
e_{31} (C/m^2)	-0.13
e_{32} (C/m^2)	-0.45
e_{24} (C/m^2)	-0.276
e_{15} (C/m^2)	-0.009
d_{33} (Ns/CV)	-46×10^{-12}
μ_{33} (Ns^2/C^2)	12.5664×10^{-7}
$s_{11}=s_{22}=s_{33}$ (C/Vm)	16×10^{-9}

in which:

$$\{d\}=\left\{\bar{u},\bar{v},\bar{w},\bar{\varphi}_1,\bar{\varphi}_2,\bar{\phi},\bar{\psi}\right\}^T\tag{60}$$

The components of [K], [M] and [C] matrices are given in "Appendix B". In order to determine the natural frequencies of the shell, the eigenvalue problem of Eq. (59) should be solved.

5. Results and discussion

5.1 Validation of the results

The results for free vibration of MEE FG-CNTRC thick cylindrical shell are presented in this section. The MEE composite shell is made up from PVDF which is reinforced by CNTs. The temperature-independent properties and the efficiency parameters of CNTs and also the temperature-independent properties of PVDF are presented in Tables 1-3.

The temperature-dependent properties of CNTs and its coefficients are listed in Tables 4 and 5.

Table 4 Temperature-dependent material properties of CNTs (Jooybar *et al*. 2016)

T (*Kelvin*)	E_{11} (*TPa*)	E_{22} (*TPa*)	G_{12} (*TPa*)
300	5.6466	7.0800	1.9445
500	5.5308	6.9348	1.9643
700	5.4744	6.8641	1.9644
1000	5.2814	6.6220	1.9451

Table 5 Coefficients of temperature-dependent material properties for CNTs (X_{0ij}=X_{ij} at 300 K) (Jooybar *et al*. 2016)

	P_0	P_1	P_2	P_3
E_{11}/E_{011}	1	-1.5849×10^{-4}	3.5390×10^{-7}	-3.7070×10^{-10}
E_{22}/E_{022}	1	-1.5852×10^{-4}	3.5408×10^{-7}	-3.7090×10^{-10}
G_{12}/G_{012}	1	8.3093×10^{-5}	-1.7803×10^{-7}	8.5651×10^{-11}

Table 6 Temperature-dependent material properties of PVDF (Laiarinandrasana *et al*. 2009)

T (°C)	E (*GPa*)	v
-50	3.5	0.384
-30	3	0.384
-20	2.8	0.384
-10	2.6	0.384
0	2.4	0.384
20	2	0.384

Table 7 The natural frequencies (Hz) for a cylindrical panel. (L=5.0 m, R=1.0 m, h= 0.01 m, E_x= 120 *GPa*, E_y= 10 *GPa*, G_{xy}= 5.5 *GPa*, ρ= 1700 kg/m^3, v_y= 0.27, n=1)

	m					
	1	2	3	4	5	6
Liu *et al*. 2012 (S-DQFME)	741	416	258	198	209	266
Liu *et al*. 2012 (Exact)	741	416	258	198	209	266
Greenberg & Stavsky 1980	765	430	266	202	211	270
Mohammadimehr *et al*. 2018b	725	-	-	-	-	-
Present study	741.324-415.846-256.596-194.350-203.539-259.921					

Fig. 3a shows the variation of mechanical properties of CNTs versus temperature according to Eq. (12). It's seen that increasing the temperature caused smooth decreasing in mechanical properties of CNTs. In Table 6 the temperature-dependent properties of PVDF are seen and Fig. 3b shows the effect of temperature variations on properties of PVDF according to Eq. (13).

By comparison Figs. 3a and b, it can be found that PVDF mechanical properties depend on temperature more than CNTs.

To validate the results, firstly the frequencies of a cylindrical panel are obtained and presented in Table 7.

The results show a good agreement between the present results and previous studies, especially in the lower modes. In addition, the results for CNTRC panel are obtained and

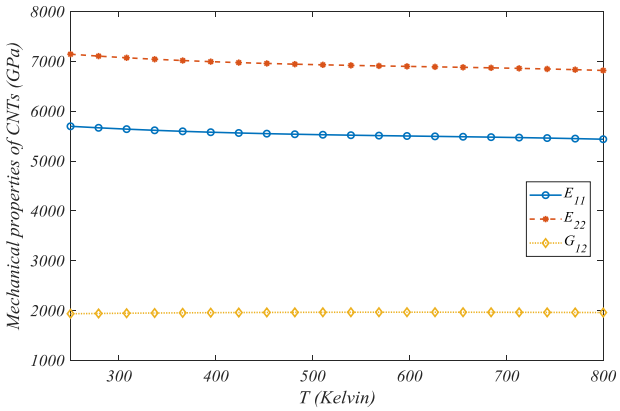

(a)

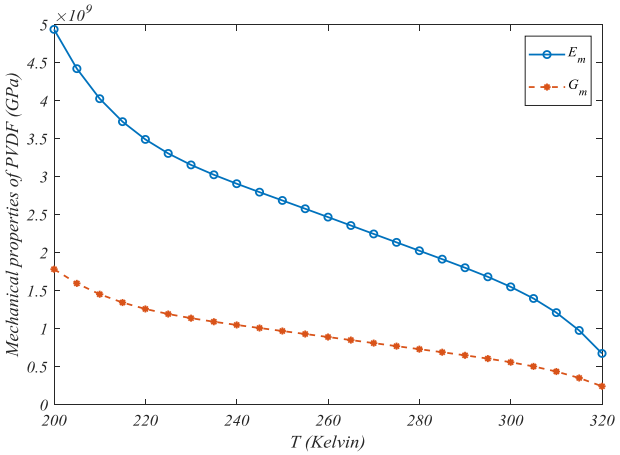

(b)

Fig. 3. Effect of temperature variations on mechanical properties of a) CNTs; b) PVDF

compared with those of Shen and Xiang (2014) in Table 8. The natural frequencies are given in this table for different volume fractions and CNTs distribution patterns. In this case, also the results have good agreement with the previous one, so the reliability of the present study results is verified. Accordingly, the results of the present research will be obtained in the following.

5.2 Parametric study

A detailed case study is presented to consider the effects of different parameters such as CNTs volume fraction variations, various CNTs distribution types, temperature variations, aspect ratios, viscoelastic foundation parameters, orientation angle, electro-magnetic potentials and wave numbers in axial and circumferential directions on natural frequencies. Also, a comparison between FSD and TSD theories results are presented in some cases. It is noted that by setting c_1 is equal to zero, the equations and results are obtained based on FSDT.

Fig. 4a and b show the effect of temperature variations on the frequency of two patterns of CNTs distribution i.e. *UD* and *FG-V*. By increasing the temperature, as shown in Fig. 3a and b the stiffness of the structure will be reduced and since the frequency is generally related to the root of ratio of stiffness to density, it decreases, as seen in Figs. 4a

Table 8 The natural frequencies of a FG-CNTRC cylindrical panel (L=R=2 cm, h= 0.1 cm, ϕ_r= 1 rad ($\Omega=\omega[(R\phi_r)^2/h]\sqrt{(\rho_m/E_m)}$)

Distribution pattern		V^*_{CNT}	(m,n) (1,1)	(2,1)	(1,2)	(2,2)
UD	Shen and Xiang (2014)	0.12	18.5407	21.0260	49.3244	50.0089
		0.17	23.0831	26.4252	61.8074	62.7873
		0.28	26.5256	29.6410	69.6560	70.4044
	Present study	0.12	17.9196	20.6091	48.5177	49.4781
		0.17	22.3094	25.8875	60.8132	62.1155
		0.28	25.6388	29.0766	68.4888	69.6662
FG-V	Shen and Xiang (2014)	0.12	17.1701	19.8495	45.6217	46.5280
		0.17	21.4163	25.0139	56.8414	58.1277
		0.28	24.4865	27.9233	65.0400	66.0279
	Present study	0.12	16.2408	19.0724	44.7678	45.7315
		0.17	20.2374	24.0801	55.8335	57.1777
		0.28	23.6196	27.2616	64.1162	65.4257
FG-A	Shen and Xiang (2014)	0.12	17.0885	20.4248	47.3984	52.8486
		0.17	21.1943	25.5235	58.8255	65.2632
		0.28	24.9235	29.3936	68.3134	76.8264
	Present study	0.12	16.5416	19.5730	44.7566	46.1010
		0.17	20.6176	24.6564	55.7308	57.5732
		0.28	23.5909	27.4804	63.7875	65.2758
FG-X	Shen and Xiang (2014)	0.12	22.0781	26.1749	56.9005	66.2032
		0.17	27.3541	32.7020	71.2389	82.7012
		0.28	32.1718	38.7997	79.1357	94.2125
	Present study	0.12	19.8521	22.5305	52.2571	53.2012
		0.17	24.7420	28.4712	65.5765	66.9202
		0.28	28.3729	32.4865	72.0374	73.5316

and b that the natural frequency is a decreasing function of temperature. Also by comparing these two figures, it can be found that the natural frequency of the *UD* is more than *FG-V*. Also, it is seen that the radius to thickness ratio (R/h) has a significant impact on the natural frequency. As the R/h ratio increases, the natural frequency will be reduced due to reducing the stiffness of the plate.

Table 9 illustrates the frequency of different vibration modes. The results of this table are for the room temperature, in the absence of elastic foundation and are for five mentioned CNTs distribution patterns. By enhancement the CNTs volume fraction, the stiffness of the shell will be increased due to high elasticity modulus of CNTs, so the frequency leads to increases. Comparing different CNTs distribution patterns shows that the *FG-X* pattern has the most values of the frequency because of this in this type, the CNTs are more in the surfaces of the shell rather than the mid-surface. But in *FG-O* distribution, the CNTs are more distributed in around of mid-surface that there isn't any strain there. Consequently, the most and the least values of the natural frequencies are respectively for *FG-X* and *FG-O* patterns. For other patterns of FG distribution of CNTs a similar thing happens.

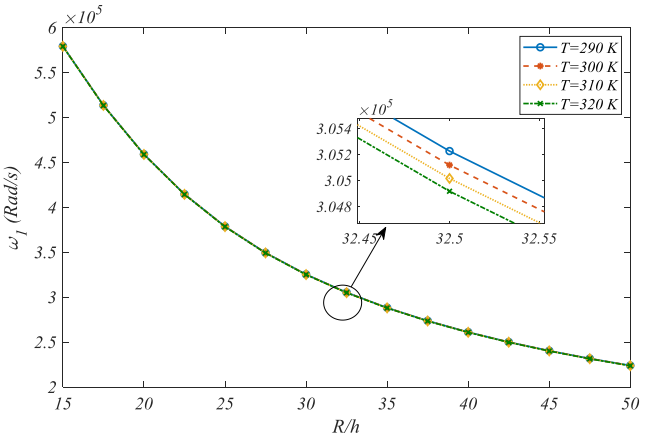

(a)

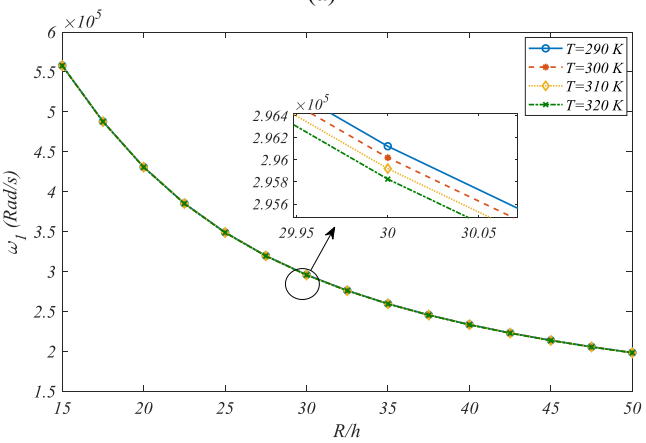

(b)

Fig. 4 Effect of Temperature variations on the fundamental natural frequency of the MEE FG-CNTRC Cylindrical circular shell for a) *UD*; b) *FG-V* CNTs distribution. (L=1.92 cm)

Table 9 The Dimensionless natural frequencies of an MEE FG-CNTRC thick circular cylindrical shell (R/L=2, R=3.84 cm, h=1 cm)

Distribution pattern	V^*_{CNT}	(m,n) (1,1) $\times10^3$	(2,1) $\times10^3$	(1,2) $\times10^3$	(2,2) $\times10^3$	(1,3) $\times10^3$	(2,3) $\times10^3$
UD	0.12	5.2945	5.4627	10.491	10.582	15.707	15.768
	0.17	6.9154	7.1361	13.704	13.823	20.517	20.597
	0.28	7.4184	7.6527	14.703	14.829	22.014	22.098
FG-V	0.12	5.2732	5.3525	10.499	10.556	15.727	15.767
	0.17	6.9045	6.9886	13.756	13.823	20.606	20.654
	0.28	7.5360	7.5955	15.020	15.072	22.487	22.529
FG-A	0.12	4.8862	5.3535	10.523	10.610	15.753	15.807
	0.17	6.2603	6.2973	13.800	13.916	20.659	20.732
	0.28	7.3530	7.3967	15.027	15.212	22.536	22.106
FG-X	0.12	5.3101	5.4748	10.566	10.735	15.786	15.886
	0.17	6.9639	7.1805	13.923	14.240	20.724	20.888
	0.28	7.6180	7.8443	15.097	15.702	22.609	22.695
FG-O	0.12	4.3121	4.4852	9.525	9.618	14.757	14.821
	0.17	5.9655	5.1940	12.802	12.925	19.664	19.747
	0.28	6.6219	6.8729	14.106	14.241	21.617	21.709

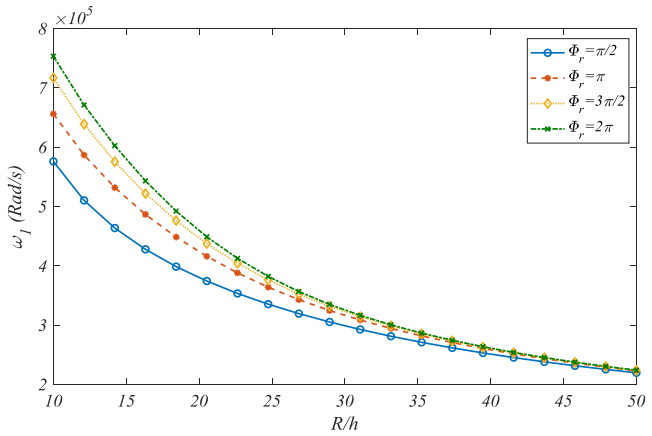

(a)

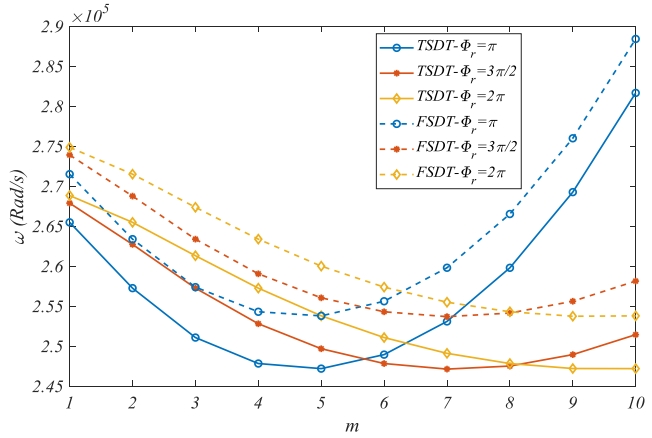

(b)

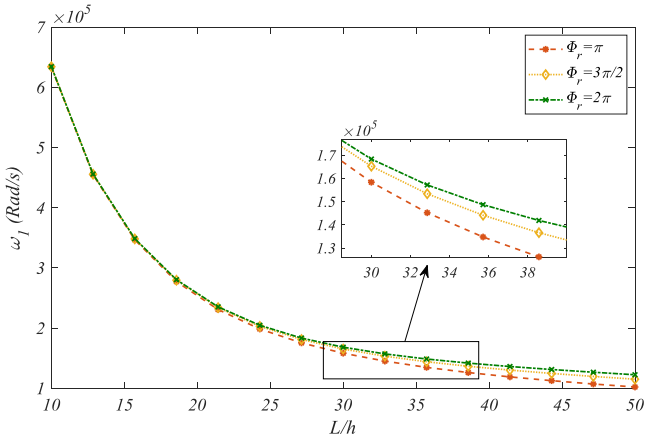

(c)

Fig. 5 Effect of orientation angle variations on the fundamental natural frequency of Magneto electro elastic thick cylindrical panel for a) *R/h* ratio variations; b) axial half sine wave number and both FSD and TSD theories; c) *L/h* ratio variations. (*n*=1)

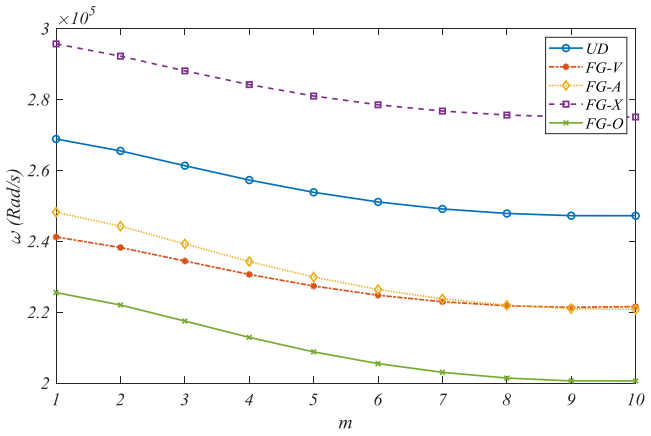

Fig. 6 Effect of various types of CNTs distribution and axial half sine wave number (*m*) on the fundamental natural frequency (*n*= 1)

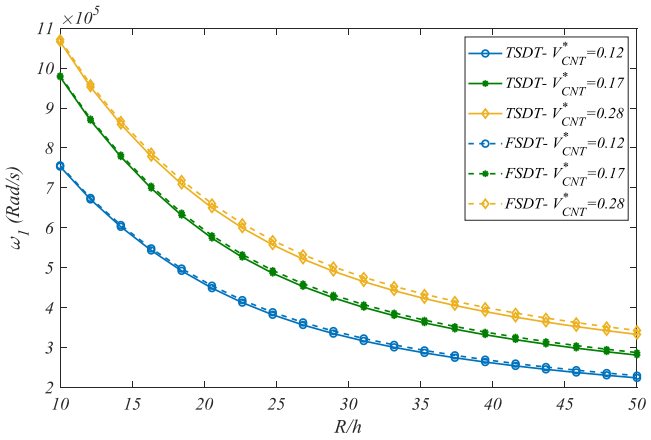

(a)

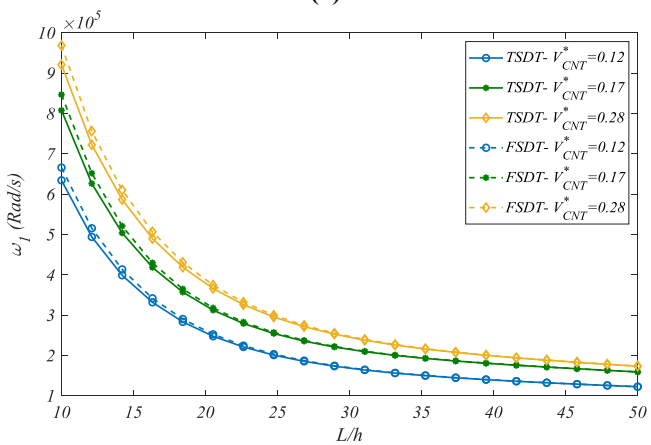

(b)

Fig. 7 Comparing the FSD and TSD theories results on the influence of V_{CNT}^{*} on the natural frequency of MEE FG-CNTRC shell versus a) *R*-to-*h* ratio; b) *L*-to-*h* ratio

Fig. 5a shows the effect of orientation angle on the results. It is seen that as the panel cross-section becomes circular, the natural frequency raises and Fig. 5b illustrates the effect of the axial wave number (*m*) variations on the results for both of FSD and TSD theories. Although the frequency reduced in the first numbers of axial wave number, it increases after a specific value of *m*. Also the decreasing rate of frequency with regard to *R/h* ratio, for the higher orientation angle is more than lower ones. This fact can be found by comparing different orientation angle and their slope. Fig. 5b also depicts that the obtained results based on FSDT have higher values rather than those of TSDT due to higher accuracy of TSDT. In Fig. 5c, it is seen

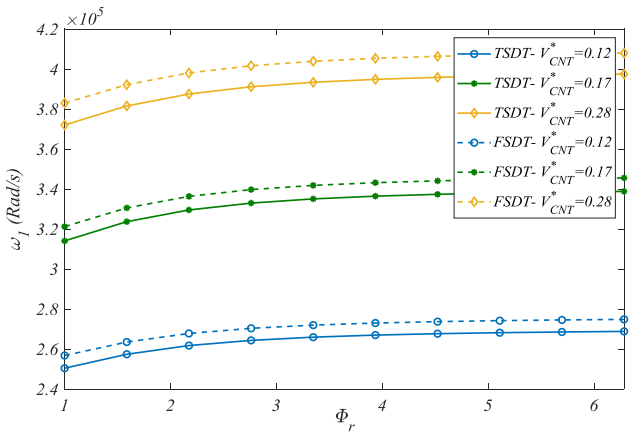

Fig. 8 Effect of orientation angle variations and CNTs volume fraction on the fundamental frequency for TSD and FSD theories. (R/L=2, m=n= 1)

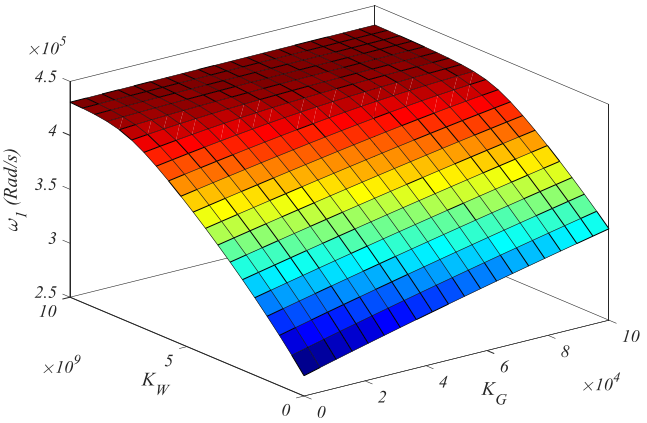

Fig. 9 Effect of Winkler-Pasternak elastic foundation parameters on the fundamental natural frequency of cylindrical circular shell. (R/L=2)

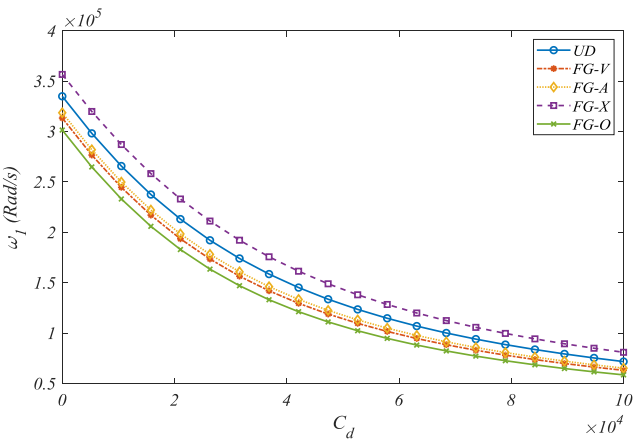

(a)

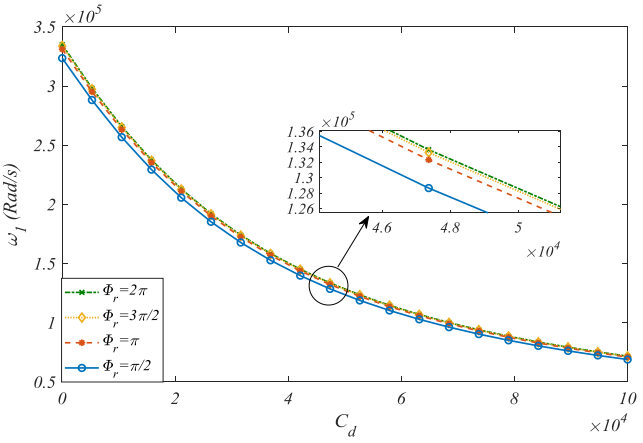

(b)

Fig. 10 Effect of damping constant of elastic foundation on the natural frequency of the shell for a) various types of CNTs distribution; b) different orientation angle. (K_W=10e6, K_G=10e4)

that as the shell becomes more cylinder, the frequency decreases. By increasing the aspect ratio of the shell, the stiffness will be reduced and so the frequency decreases. Fig. 5 is presented for UD, V^*_{CNT} =0.12 and room temperature.

Fig. 6 is comparing different FG distribution patterns of CNTs respect to half axial sine wave number and it confirms the previous statements that the *FG-X* has the maximum and *FG-O* has the minimum values of the frequencies. This figure is plotted for the circular cross-section, V^*_{CNT} =0.12 and the room temperature.

Influence of increasing volume fraction of CNTs for both FSD and TSD theories versus R/h and L/h ratio is presented in Figs. 7a and b. It is found that as stated before, due to the high elastic modulus of CNTs, their increasing will leads the stiffness and following it, the frequency of the structure to increase. Also, it can be concluded that the TSDT results for thicker states are more accurate rather than FSDT, while their difference in the shell with low thickness is negligible.

Fig. 8 shows the effect of orientation angle increasing on the fundamental natural frequency.

The results that have been presented so far are in absence of viscoelastic foundation but in Fig. 9 the effect of Pasternak foundation on the natural frequency of the shell is considered. This figure depicts the effect of both Winkler or spring constant and Pasternak or shear layer constant simultaneously. It is seen that enhancement both of the mentioned constants, will increase the stability and rigidity of the shell and reduce its vibrations, so its frequency leads to higher values. Also, it can be found that the effect of Pasternak constant is more than that of Winkler.

Effect of damping constant is presented in Fig. 10. Fig. 10a shows this effect for various patterns of CNTs distribution and Fig. 10b shows it for different orientation angle of the cross-section. Both of the mentioned figures indicate that unlike the Winkler and Pasternak constants, by enhancing the viscous constant, the structure's rigidity reduces and following it the vibration of the shell increases.

Fig. 11 compares different types of elastic foundation and depicts the effect of them on the vibrational behavior of the shell. As it can be seen in this figure, the Winkler-Pasternak foundation has the most stability and vice versa, the visco-Winkler has the least. It means adding the viscoelastic foundation to the structure will increase its vibrations. But regardless of the viscous models, it can be

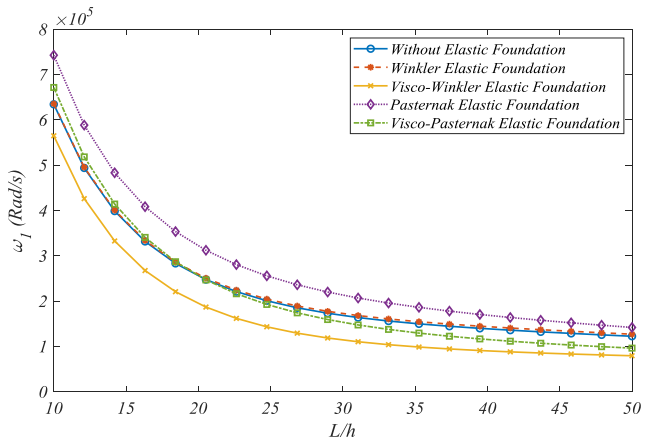

Fig. 11 Comparing effect of different models of elastic foundation on the results

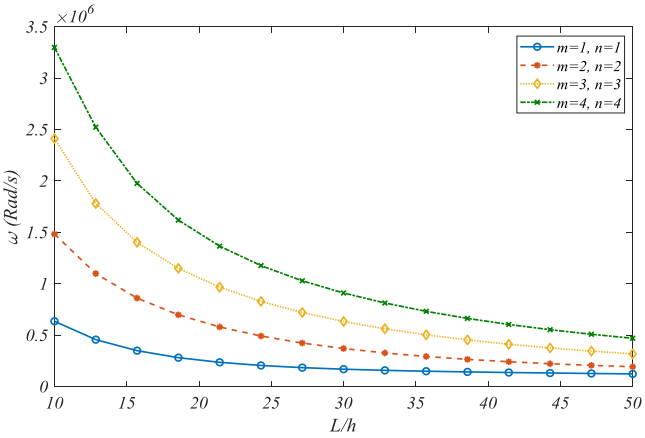

(a)

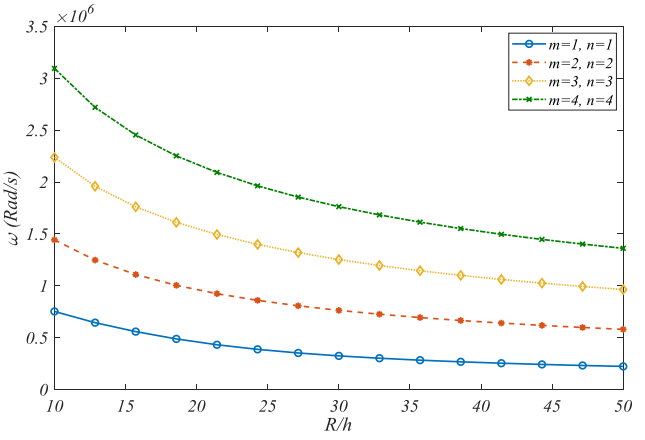

(b)

Fig. 12 Effect of different values of (m, n) on the fundamental frequency of the structure versus a) length to thickness ratio; b) radius to thickness ratio. (R/L=2)

concluded adding the elastic foundation generally can be reduced the vibrations of the structure and consequently the frequencies are raising.

In Figs. 12a, and b, the natural frequencies of first for vibrational modes are plotted respect to L/h and R/h ratios. As it can be expected the influence of L/h and R/h ratios variations on the higher modes are more than the lower

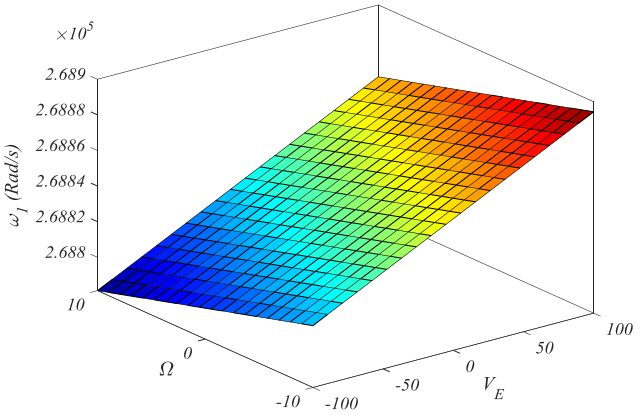

Fig. 13 Effect of electric and magnetic potentials on the natural frequency of the MEE FG-CNTRC cylindrical circular shell

ones. This can be found by noting the slope of the curves.

Effect of applied electric and magnetic potentials is investigated in Fig. 13 simultaneously. Although the frequency is an increasing function of electric potential, it is seen that increasing the magnetic potential, leads the natural frequency to decrease. So electric and magnetic potentials manner are different from each other.

6. Conclusions

The present study investigated vibrational behavior of MEE composite cylindrical shell which was reinforced by CNTs and was rested on visco-Pasternak elastic foundation. The matrix of the composite shell was made up of PVDF and the composite properties were assumed to be varied by temperature variations. Since the shell was thick, TSDT was used to describe the displacement components and based on Hamilton's principle and variational formulation the motion equations were obtained and solved via Navier's method for the simply supported ends shell and effect of different parameters such as temperature variations, orientation angle variations, increasing CNTs volume fractions, various patterns for CNTs distribution, axial and circumferential wave numbers, L/h and R/h ratios, electro-magnetic potentials and adding viscoelastic foundation to the structure were considered and the following results were obtained:

- By temperature raising, due to decreasing the stiffness of the nano-composite, and because of the direct relationship between frequency and stiffness, the natural frequency of the shell decreases.
- Enhancement of CNTs volume fraction leads to increase the stiffness and the frequency.
- By comparing different patterns of CNTs FG distribution, it is found *FG-X* pattern has the most values of frequency and *FG-O* has the least ones. Since in *FG-X* the CNTs are more in the exterior and interior surfaces of the shell, so its frequency increases, but for *FG-O* pattern, the CNTs are distributed more around mid-surface.
- As the radius of the shell respect to its thickness

increases leads the frequency to decrease.

- As the shell becomes more cylinder the frequency decreases.
- By increasing the orientation angle of the panel, the frequency increases. So the circular shell has the lowest value of the frequency.
- Increasing axial wave number leads the frequency to increases.
- Adding elastic foundation enhances the stiffness of the shell and so the frequency increases.
- Increasing damping constant reduces the stiffness and natural frequency of the structure.
- As the shell becomes thicker, TSDT presents more accurate results rather than FSDT.
- Unlike the electric potential, increasing the magnetic potential lead the frequency to reduce.

Acknowledgment

The authors would like to thank the referees for their valuable comments. Also, they are thankful to the Iranian Nanotechnology Development Committee for their financial support and the University of Kashan for supporting this work by Grant No. 682561/16.

References

Abdel-Rahman, E.M., Younis, M.I. and Nayfeh, A.H. (2002), "Characterization of the mechanical behavior of an electrically actuated microbeam", *J. Micromech. Microeng.*, **12**(6), 759.

Alibeigloo, A. (2014), "Three-dimensional thermoelasticity solution of functionally graded carbon nanotube reinforced composite plate embedded in piezoelectric sensor and actuator layers", *Compos. Struct.*, **118**, 482-495. https://doi.org/10.1016/j.compstruct.2014.08.004.

Amir, S. (2016), "Orthotropic patterns of visco-Pasternak foundation in nonlocal vibration of orthotropic graphene sheet under thermo-magnetic fields based on new first-order shear deformation theory", *Proceedings of the Institution of Mechanical Engineers, Part L: Journal of Materials: Design and Applications*, https://doi.org/10.1177/2F1464420716670929.

Amir, S., Bidgoli, E.M.R. and Arshid, E. (2018), "Size-dependent vibration analysis of a three-layered porous rectangular nano plate with piezo-electromagnetic face sheets subjected to pre loads based on SSDT", *Mech. Adv. Mater. Struct.*, 1-15. https://doi.org/10.1080/15376494.2018.1487612.

Amir, S., Khani, M., Shajari, A.R. and Dashti, P. (2017), "Instability analysis of viscoelastic CNTs surrounded by a thermo-elastic foundation", *Strcut. Eng. Mech.*, **63**(2), 171-180. https://doi.org/10.12989/sem.2017.63.2.171.

Ansari, R. and Gholami, R. (2016), "Nonlocal free vibration in the pre-and post-buckled states of magneto-electro-thermo elastic rectangular nanoplates with various edge conditions", *Smart Mater. Struct.*, **25**(9), 95033.

Aragh, B. S., Barati, A. H. N. and Hedayati, H. (2012), "Eshelby-Mori-Tanaka approach for vibrational behavior of continuously graded carbon nanotube-reinforced cylindrical panels", *Compos. Part B*, **43**(4), 1943-1954. https://doi.org/10.1016/j.compositesb.2012.01.004.

Arefi, M., Bidgoli, E.M.R. and Zenkour, A.M. (2018), "Size-dependent free vibration and dynamic analyses of a sandwich microbeam based on higher-order sinusoidal shear deformation theory and strain gradient theory", *Smart Struct. Syst.*, **22**(1), 27-40.

Arshid, E. and Khorshidvand, A.R. (2017), "Flexural vibrations analysis of saturated porous circular plates using differential quadrature method", *Iran J. Mech. Eng. Transac. ISME*, **19**(1), 78-100.

Arshid, E. and Khorshidvand, A.R. (2018), "Free vibration analysis of saturated porous FG circular plates integrated with piezoelectric actuators via differential quadrature method", *Thin Wall. Struct.*, **125**(January), 220-233. https://doi.org/10.1016/j.tws.2018.01.007.

Arshid, E., Kiani, A. and Amir, S. (2019), "Magneto-electro-elastic vibration of moderately thick FG annular plates subjected to multi physical loads in thermal environment using GDQ method by considering neutral surface", *Proceedings of the Institution of Mechanical Engineers, Part L: Journal of Materials: Design and Applications*. https://doi.org/10.1177/1464420719832626.

Ashrafi, B., Hubert, P. and Vengallatore, S. (2006), "Carbon nanotube-reinforced composites as structural materials for microactuators in microelectromechanical systems", *Nanotechnol.*, **17**(19), 4895.

Belmahi, S., Zidour, M., Meradjah, M., Bensattalah, T. and Dihaj, A. (2018), "Analysis of boundary conditions effects on vibration of nanobeam in a polymeric matrix", *Struct. Eng. Mech.*, **67**(5), 517-525. https://doi.org/10.12989/sem.2018.67.5.517.

Bennoun, M., Houari, M.S.A. and Tounsi, A. (2016), "A novel five-variable refined plate theory for vibration analysis of functionally graded sandwich plates", *Mech. Adv. Mater. Struct.*, **23**(4), 423-431. https://doi.org/10.1080/15376494.2014.984088.

Bhardwaj, G., Singh, I.V., Mishra, B.K. and Bui, T.Q. (2015), "Numerical simulation of functionally graded cracked plates using NURBS based XIGA under different loads and boundary conditions", *Compos. Struct.*, **126**, 347-359. https://doi.org/10.1016/j.compstruct.2015.02.066.

Bui, T.Q., Do, T.V., Ton, L.H.T., Doan, D.H., Tanaka, S., Pham, D.T. and Hirose, S. (2016), "On the high temperature mechanical behaviors analysis of heated functionally graded plates using FEM and a new third-order shear deformation plate theory", *Compos. Part B*, **92**, 218-241. https://doi.org/10.1016/j.compositesb.2016.02.048.

Cong, P. H., Chien, T. M., Khoa, N. D. and Duc, N. D. (2018), "Nonlinear thermomechanical buckling and post-buckling response of porous FGM plates using Reddy's HSDT", *Aerosp. Sci. Technol.*, **77**, 419-428. https://doi.org/10.1016/j.ast.2018.03.020.

Das, Y. C. (1964), "Vibrations of orthotropic cylindrical shells", *Applied Scientific Research, Section A*, **12**(4-5), 317-326. https://doi.org/10.1007/BF03185004.

Dong, S.B. (1968), "Free vibration of laminated orthotropic cylindrical shells", *J. Acoustic. Soc. America*, **44**(6), 1628-1635. https://doi.org/10.1121/1.1911306.

Duc, N.D. and Quan, T.Q. (2015), "Nonlinear dynamic analysis of imperfect functionally graded material double curved thin shallow shells with temperature-dependent properties on elastic foundation", *J. Vib. Control*, **21**(7), 1340-1362. https://doi.org/10.1177/1077546313494114.

El-Haina, F., Bakora, A., Bousahla, A.A., Tounsi, A. and Mahmoud, S.R. (2017), "A simple analytical approach for thermal buckling of thick functionally graded sandwich plates", *Struct. Eng. Mech.*, **63**(5), 585-595. https://doi.org/10.12989/sem.2017.63.5.585.

Forsberg, K. (1964), "Influence of boundary conditions on the modal characteristics of thin cylindrical shells", *AIAA J.*, **2**(12), 2150-2157. https://doi.org/10.2514/3.55115.

Ganesan, N. and Sivadas, K.R. (1990), "Vibration analysis of orthotropic shells with variable thickness", *Comput. Struct.*,

35(3), 239-248. https://doi.org/10.1016/0045-7949(90)90343-Z.
Ghorbanpour Arani, A., Haghparast, E. and BabaAkbar-Zarei, H. (2017a), "Vibration analysis of functionally graded nanocomposite plate moving in two directions", *Steel Compos. Struct.*, **23**(5), 529-541. https://doi.org/10.12989/scs.2017.23.5.529.
Ghorbanpour Arani, A., Roudbari, M.A. and Amir, S. (2016a), "Longitudinal magnetic field effect on wave propagation of fluid-conveyed SWCNT using Knudsen number and surface considerations", *Appl. Math. Model.*, **40**(3), 2025-2038. https://doi.org/10.1016/j.apm.2015.09.055.
Ghorbanpour Arani, A., Maraghi, Z.K. and Ferasatmanesh, M. (2017b), "Theoretical investigation on vibration frequency of sandwich plate with PFRC core and piezomagnetic face sheets under variable in-plane load", *Struct. Eng. Mech.*, **63**(1), 65-76. https://doi.org/10.12989/sem.2017.63.1.065.
Ghorbanpour Arani A., Mohammadimehr M., Saidi A. R., Shogaei S. and Arefmanesh A. (2011a), "Thermal buckling analysis of double-walled carbon nanotubes considering the small-scale length effect", *Proc. IMechE, Part C, J. Mech. Eng. Sci*., **225** (1), 248-256. https://doi.org/10.1177/09544062JMES1975.
Ghorbanpour Arani A., Hashemian M., Loghman A. and Mohammadimehr M. (2011b), "Study of dynamic stability of the double-walled carbon nanotubes under axial loading embedded in an elastic medium by the energy method", *J. Appl. Mech. Technical Physics*, **52**(5), 815-824. https://doi.org/10.1134/S0021894411050178.
Ghorbanpour Arani, A., Mobarakeh, M.R., Shams, S. and Mohammadimehr, M. (2012), "The effect of CNT volume fraction on the magneto-thermo-electro-mechanical behavior of smart nanocomposite cylinder", *J. Mech. Sci. Technol.*, **26**(8), 2565-2572. https://doi.org/10.1007/s12206-012-0639-5.
Ghorbanpour Arani, A., BabaAkbar-Zarei, H., Pourmousa, P. and Eskandari, M. (2018a), "Investigation of free vibration response of smart sandwich micro-beam on Winkler-Pasternak substrate exposed to multi physical fields", *Microsyst. Technol.*, **24**(7), 3045-3060. https://doi.org/10.1007/s00542-017-3681-5.
Ghorbanpour Arani, A., Haghparast, E. and BabaAkbar-Zarei, H. (2016b), "Vibration of axially moving 3-phase CNTFPC plate resting on orthotropic foundation", *Struct. Eng. Mech*, **57**(1), 105-126. http://dx.doi.org/10.12989/sem.2016.57.1.105.
Ghorbanpour Arani, A. and Kiani, F. (2018b), "Nonlinear free and forced vibration analysis of microbeams resting on the nonlinear orthotropic visco-Pasternak foundation with different boundary conditions", *Steel Compos. Struct.*, **28**(2), 149-165. https://doi.org/10.12989/scs.2018.28.2.149.
Ghorbanpour Arani, A., Kiani, F. and Afshari, H. (2019), "Free and forced vibration analysis of laminated functionally graded CNT-reinforced composite cylindrical panels", *J. Sandwich Struct. Mater.*, 1099636219830787. https://doi.org/10.1177/1099636219830787.
Ghorbanpour Arani, A., Pourjamshidian, M. and Arefi, M. (2018c), "Non-linear free and forced vibration analysis of sandwich nano-beam with FG-CNTRC face-sheets based on nonlocal strain gradient theory", *Smart Struct. Syst.*, **22**(1), 105-120.
Greenberg, J.B. and Stavsky, Y. (1980), "Buckling and vibration of orthotropic composite cylindrical shellsBeul-und Schwingverhalten kompositer, orthotroper, zylindrischer Schalen", *Acta Mechanica*, **36**(1-2), 15-29. https://doi.org/10.1007/BF01178233.
Hu, W.C.L. (1964), "A survey of the literature on the vibrations of thin shells", NASA-CR-58048; Southwest Research InsL, San Antonio, USA.
Iijima, S. (1991), "Helical microtubules of graphitic carbon", *Nature*, **354**(6348), 56. https://doi.org/10.1038/354056a0.
Jam, J.E., Pourasghar, A. and Kamarian, S. (2012), "Effect of the aspect ratio and waviness of carbon nanotubes on the vibrational behavior of functionally graded nanocomposite cylindrical panels", *Polym. Compos.*, **33**(11), 2036-2044.
Jooybar, N., Malekzadeh, P. and Fiouz, A. (2016), "Vibration of functionally graded carbon nanotubes reinforced composite truncated conical panels with elastically restrained against rotation edges in thermal environment", *Compos. Part B*, **106**, 242-261. https://doi.org/10.1016/j.compositesb.2016.09.030.
Laiarinandrasana, L., Besson, J., Lafarge, M. and Hochstetter, G. (2009), "Temperature dependent mechanical behaviour of PVDF: experiments and numerical modelling", *J. Plasticity*, **25**(7), 1301-1324. https://doi.org/10.1016/j.ijplas.2008.09.008.
Lang, Z. and Xuewu, L. (2013), "Buckling and vibration analysis of functionally graded magneto-electro-thermo-elastic circular cylindrical shells", *Appl. Math. Model.*, **37**(4), 2279-2292. https://doi.org/10.1016/j.apm.2012.05.023.
Leissa, A. W. (1973), *Vibration of Shells* (Vol. 288), Scientific and Technical Information Office, National Aeronautics and Space Administration Washington. USA.
Liu, B., Xing, Y.F., Qatu, M.S. and Ferreira, A.J.M. (2012), "Exact characteristic equations for free vibrations of thin orthotropic circular cylindrical shells", *Compos. Struct.*, **94**(2), 484-493. https://doi.org/10.1016/j.compstruct.2011.08.012.
Liu, P., Bui, T.Q., Zhu, D., Yu, T.T., Wang, J.W., Yin, S.H. and Hirose, S. (2015), "Buckling failure analysis of cracked functionally graded plates by a stabilized discrete shear gap extended 3-node triangular plate element", *Compos. Part B*, *77*, 179-193. https://doi.org/10.1016/j.compositesb.2015.03.036.
Liu, S., Yu, T. and Bui, T.Q. (2017), "Size effects of functionally graded moderately thick microplates: A novel non-classical simple-FSDT isogeometric analysis", *Europ. J. Mech. A*, **66**, 446-458. https://doi.org/10.1016/j.euromechsol.2017.08.008.
Liu, S., Yu, T., Lich, L. Van, Yin, S. and Bui, T.Q. (2019), "Size and surface effects on mechanical behavior of thin nanoplates incorporating microstructures using isogeometric analysis", *Comput. Struct.*, **212**, 173-187. https://doi.org/10.1016/j.compstruc.2018.10.009.
Liu, S., Yu, T., Van Lich, L., Yin, S. and Bui, T. Q. (2018), "Size effect on cracked functional composite micro-plates by an XIGA-based effective approach", *Meccanica*, **53**(10), 2637-2658. https://doi.org/10.1007/s11012-018-0848-9.
Loja, M.A.R., Soares, C.M.M. and Barbosa, J.I. (2014), "Optimization of magneto-electro-elastic composite structures using differential evolution", *Compos. Struct.*, **107**, 276-287. https://doi.org/10.1016/j.compstruct.2013.08.005.
Malekzadeh, P. and Shojaee, M. (2013), "Buckling analysis of quadrilateral laminated plates with carbon nanotubes reinforced composite layers", *Thin Wall. Struct.*, **71**, 108-118. https://doi.org/10.1016/j.tws.2013.05.008.
Mehar, K., Panda, S. K., Bui, T. Q. and Mahapatra, T. R. (2017), "Nonlinear thermoelastic frequency analysis of functionally graded CNT-reinforced single/doubly curved shallow shell panels by FEM", *J. Therm. Stress*, **40**(7), 899-916. https://doi.org/10.1080/01495739.2017.1318689.
Meksi, A., Benyoucef, S., Houari, M. S. A. and Tounsi, A. (2015), "A simple shear deformation theory based on neutral surface position for functionally graded plates resting on Pasternak elastic foundations", *Struct. Eng. Mech.*, **53**(6), 1215-1240.
Mohammadimehr, M., Akhavan Alavi, S. M., Okhravi, S. V and Edjtahed, S. H. (2018a), "Free vibration analysis of micro-magneto-electro-elastic cylindrical sandwich panel considering functionally graded carbon nanotube-reinforced nanocomposite face sheets, various circuit boundary conditions, and temperature-dependent material properties using high-order sandwich panel theory and modified strain gradient theory", *J. Intelligent Mater. Syst. Struct.*, **29**(5), 863-882. https://doi.org/10.1177/1045389X17721048.

Mohammadimehr, M., Emdadi, M. and Rousta Navi, B. (2018c), "Dynamic stability analysis of microcomposite annular sandwich plate with carbon nanotube reinforced composite facesheets based on modified strain gradient theory", *J. Sandwich Struct. Mater.*, https://doi.org/10.1177/1099636218782770.

Mohammadimehr, M., Mohandes, M. and Moradi, M. (2016a), "Size dependent effect on the buckling and vibration analysis of double-bonded nanocomposite piezoelectric plate reinforced by boron nitride nanotube based on modified couple stress theory", *J. Vib. Control*, **22**(7), 1790-1807. https://doi.org/10.1177/1077546314544513.

Mohammadimehr, M., Moradi, M. and Loghman, A. (2014), "Influence of the elastic foundation on the free vibration and buckling of thin-walled piezoelectric-based FGM cylindrical shells under combined loadings", *J. Solid Mech*, **6**(4), 347-365.

Mohammadimehr, M. and Mostafavifar, M. (2016), "Free vibration analysis of sandwich plate with a transversely flexible core and FG-CNTs reinforced nanocomposite face sheets subjected to magnetic field and temperature-dependent material properties using SGT", *Compos. Part B*, **94**, 253-270. https://doi.org/10.1016/j.compositesb.2016.03.030.

Mohammadimehr, M., Rousta Navi, B. and Arani, A.G. (2015), "Free vibration of viscoelastic double-bonded polymeric nanocomposite plates reinforced by FG-SWCNTs using MSGT, sinusoidal shear deformation theory and meshless method", *Compos. Struct.*, **131**, 654-671.

Mohammadimehr, M., Rousta Navi, B. and Arani, A.G. (2016b), "Modified strain gradient Reddy rectangular plate model for biaxial buckling and bending analysis of double-coupled piezoelectric polymeric nanocomposite reinforced by FG-SWNT", *Compos. Part B*, **87**, 132-148. https://doi.org/10.1016/j.compstruct.2015.05.077.

Mohammadimehr, M., Okhravi, S.V and Akhavan Alavi, S.M. (2018b), "Free vibration analysis of magneto-electro-elastic cylindrical composite panel reinforced by various distributions of CNTs with considering open and closed circuits boundary conditions based on FSDT", *J. Vib. Control*, **24**(8), 1551-1569. https://doi.org/10.1177/1077546316664022.

Mohammadimehr, M., Saidi, A.R., Ghorbanpour Arani, A., Arefmanesh, A. and Han Q. (2010), "Torsional Buckling of a DWCNT Embedded on Winkler and Pasternak Foundations Using Nonlocal Theory", *J. Mech. Sci. Tech.,* ***24***(6), 1289-1299. https://doi.org/10.1007/s12206-010-0331-6.

Mohammadimehr, M., Rousta Navi, B. and Ghorbanpour Arani, A. (2017a), "Dynamic stability of MSGT sinusoidal viscoelastic piezoelectric polymeric FG-SWNT reinforced nanocomposite plate considering surface stress and agglomeration effects under hydro-thermo-electro-magneto-mechanical loadings", *Mech. Adv. Mater. Struct.*, **24**, 1325-1342. http://dx.doi.org/10.1080/15376494.2016.1227507.

Mohammadimehr, M., Salemi, M. and Navi, B.R. (2016c), "Bending, buckling, and free vibration analysis of MSGT microcomposite Reddy plate reinforced by FG-SWCNTs with temperature-dependent material properties under hydro-thermo-mechanical loadings using DQM", *Compos. Struct.*, **138**, 361-380. https://doi.org/10.1016/j.compstruct.2015.11.055.

Mohammadimehr, M., Zarei, H. B., Parakandeh, A. and Arani, A. G. (2017b), "Vibration analysis of double-bonded sandwich microplates with nanocomposite facesheets reinforced by symmetric and un-symmetric distributions of nanotubes under multi physical fields", *Struct. Eng. Mech.*, **64**(3), 361-379. https://doi.org/10.12989/sem.2017.64.3.361.

Mohammadimehr, M., Rostami, R. and Arefi, M. (2016d), "Electro-elastic analysis of a sandwich thick plate considering FG core and composite piezoelectric layers on Pasternak foundation using TSDT", *Steel Compos. Struct.*, **20**(3), 513-544. https://doi.org/10.12989/scs.2016.20.3.513.

Mohammadimehr, M. and Rahmati, A.H. (2013), "Small scale effect on electro-thermo-mechanical vibration analysis of single-walled boron nitride nanorods under electric excitation", *Turkish J. Eng. Environ. Sci.,* **37**(1), 1-15.

Mohammadimehr M. and Shahedi S. (2017) "High-order buckling and free vibration analysis of two types sandwich beam including AL or PVC-foam flexible core and CNTs reinforced nanocomposite face sheets using GDQM", *Compos. Part B Eng.,* **108**, 91-107. https://doi.org/10.1016/j.compositesb.2016.09.040.

Nasihatgozar, M., Daghigh, V., Eskandari, M., Nikbin, K. and Simoneau, A. (2016), "Buckling analysis of piezoelectric cylindrical composite panels reinforced with carbon nanotubes", *J. Mech. Sci.*, **107**, 69-79. https://doi.org/10.1016/j.ijmecsci.2016.01.010.

Ozdemir, Y.I. (2018), "Using fourth order element for free vibration parametric analysis of thick plates resting on elastic foundation", *Struct. Eng. Mech.*, **65**(3), 213-222. https://doi.org/10.12989/sem.2018.65.3.213.

Qatu, M.S. (2002), "Recent research advances in the dynamic behavior of shells: 1989-2000, Part 1: Laminated composite shells", *Appl. Mech. Rev.*, **55**(4), 325-350. https://doi.org/10.1115/1.1483079.

Qatu, M.S. (2004), *Vibration of Laminated Shells and Plates*, Elsevier, The Netherlands.

Qatu, M.S., Sullivan, R.W. and Wang, W. (2010), "Recent research advances on the dynamic analysis of composite shells: 2000-2009", *Compos. Struct.*, **93**(1), 14-31. https://doi.org/10.1016/j.compstruct.2010.05.014.

Razavi, S. and Shooshtari, A. (2015), "Nonlinear free vibration of magneto-electro-elastic rectangular plates", *Compos. Struct.*, **119**, 377-384. https://doi.org/10.1016/j.compstruct.2014.08.034.

Reddy, J. N. (2004), *Mechanics of Laminated Composite Plates and Shells: Theory and Analysis*, CRC press, Florida, U.S.A.

Shen, H.S. (2011a), "Postbuckling of nanotube-reinforced composite cylindrical shells in thermal environments, Part I: Axially-loaded shells", *Compos. Struct.*, **93**(8), 2096-2108. https://doi.org/10.1016/j.compstruct.2011.02.011.

Shen, H.S. (2011b), "Postbuckling of nanotube-reinforced composite cylindrical shells in thermal environments, Part II: Pressure-loaded shells", *Compos. Struct.*, **93**(10), 2496-2503. https://doi.org/10.1016/j.compstruct.2011.04.005.

Shen, H.S. (2012), "Thermal buckling and postbuckling behavior of functionally graded carbon nanotube-reinforced composite cylindrical shells", *Compos. Part B*, **43**(3), 1030-1038. https://doi.org/10.1016/j.compositesb.2011.10.004.

Shen, H.S. and Xiang, Y. (2012), "Nonlinear vibration of nanotube-reinforced composite cylindrical shells in thermal environments", *Comput. Method. Appl. Mech. Eng.*, **213**, 196-205. https://doi.org/10.1016/j.cma.2011.11.025.

Shen, H.S. and Xiang, Y. (2013), "Postbuckling of nanotube-reinforced composite cylindrical shells under combined axial and radial mechanical loads in thermal environment", *Compos. Part B*, **52**, 311-322. https://doi.org/10.1016/j.compositesb.2013.04.034.

Shen, H.S. and Xiang, Y. (2014), "Nonlinear vibration of nanotube-reinforced composite cylindrical panels resting on elastic foundations in thermal environments", *Compos. Struct.*, **111**, 291-300. https://doi.org/10.1016/j.compstruct.2014.01.010.

Shen, H.S. and Zhang, C.L. (2010), "Thermal buckling and postbuckling behavior of functionally graded carbon nanotube-reinforced composite plates", *Mater. Design*, **31**(7), 3403-3411. https://doi.org/10.1016/j.matdes.2010.01.048.

Shooshtari, A. and Razavi, S. (2016), "Vibration analysis of a magnetoelectroelastic rectangular plate based on a higher-order shear deformation theory", *Latin American J. Solids Struct.*,

13(3), 554-572. http://dx.doi.org/10.1590/1679-78251831.
Smith, B.L. and Vronay, D.F. (1970), "Free vibration of circular cylindrical shells of finite length", *AIAA J.*, **8**(3), 601-603. https://doi.org/10.2514/3.5726.
Soedel, W. (1983), "Simplified equations and solutions for the vibration of orthotropic cylindrical shells", *J. Sound Vib.*, **87**(4), 555-566.
Soedel, W. (2004), *Vibrations of Shells and Plates*. CRC Press, Florida, USA.
Van Do, T., Nguyen, D. K., Duc, N. D., Doan, D. H. and Bui, T. Q. (2017), "Analysis of bi-directional functionally graded plates by FEM and a new third-order shear deformation plate theory", *Thin Wall. Struct.*, **119**, 687-699. https://doi.org/10.1016/j.tws.2017.07.022.
Vu, T. Van, Khosravifard, A., Hematiyan, M. R. and Bui, T. Q. (2018), "A new refined simple TSDT-based effective meshfree method for analysis of through-thickness FG plates", *Appl. Math. Model.*, **57**, 514-534. https://doi.org/10.1016/j.apm.2018.01.004.
Wang, Z.-X. and Shen, H.-S. (2011), "Nonlinear vibration of nanotube-reinforced composite plates in thermal environments", *Comput. Mater. Sci.*, **50**(8), 2319-2330. https://doi.org/10.1016/j.commatsci.2011.03.005.
Wang, Z.-X. and Shen, H.-S. (2012), "Nonlinear dynamic response of nanotube-reinforced composite plates resting on elastic foundations in thermal environments", *Nonlinear Dynam.*, **70**(1), 735-754. https://doi.org/10.1007/s11071-012-0491-2.
Wattanasakulpong, N. and Bui, T. Q. (2018), "Vibration analysis of third-order shear deformable FGM beams with elastic support by Chebyshev collocation method", *J. Struct. Stability Dynam.*, **18**(05), https://doi.org/10.1142/S0219455418500712.
Xuebin, L. (2006), "A new approach for free vibration analysis of thin circular cylindrical shell", *J. Sound Vib.*, **296**(1-2), 91-98. https://doi.org/10.1016/j.jsv.2006.01.065.
Yahiaoui, M., Tounsi, A., Fahsi, B., Bouiadjra, R.B. and Benyoucef, S. (2018), "The role of micromechanical models in the mechanical response of elastic foundation FG sandwich thick beams", *Struct. Eng. Mech.*, **68**(1), 53-66.
Yas, M. H., Pourasghar, A., Kamarian, S. and Heshmati, M. (2013), "Three-dimensional free vibration analysis of functionally graded nanocomposite cylindrical panels reinforced by carbon nanotube", *Mater. Design*, **49**, 583-590. https://doi.org/10.1016/j.matdes.2013.01.001.
Yin, S., Yu, T., Bui, T. Q., Liu, P. and Hirose, S. (2016a), "Buckling and vibration extended isogeometric analysis of imperfect graded Reissner-Mindlin plates with internal defects using NURBS and level sets", *Comput. Struct.*, **177**, 23-38. https://doi.org/10.1016/j.compstruc.2016.08.005.
Yin, S., Yu, T., Bui, T. Q., Zheng, X. and Tanaka, S. (2016b), "In-plane material inhomogeneity of functionally graded plates: A higher-order shear deformation plate isogeometric analysis", *Compos. Part B*, **106**, 273-284. https://doi.org/10.1016/j.compositesb.2016.09.008.
Yu, T., Bui, T. Q., Liu, P. and Hirose, S. (2016), "A stabilized discrete shear gap extended finite element for the analysis of cracked Reissner-Mindlin plate vibration problems involving distorted meshes", *J. Mech. Mater. Design*, **12**(1), 85-107. https://doi.org/10.1007/s10999-014-9282-x.
Zaoui, F. Z., Ouinas, D. and Tounsi, A. (2019), "New 2D and quasi-3D shear deformation theories for free vibration of functionally graded plates on elastic foundations", *Compos. Part B*, **159**, 231-247. https://doi.org/10.1016/j.compositesb.2018.09.051.

Appendix A

The middle plane strain components and the curvatures based on Sanders assumptions are as follows:

$$\varepsilon_{xx}^{(0)}=\frac{\partial u}{\partial x},\qquad \varepsilon_{\theta\theta}^{(0)}=\frac{1}{R}\left(\frac{\partial v}{\partial \theta}+w\right),$$
$$\gamma_{x\theta}^{(0)}=\frac{1}{R}\frac{\partial u}{\partial \theta}+\frac{\partial v}{\partial x},\qquad \gamma_{xz}^{(0)}=\varphi_1+\frac{\partial w}{\partial x},$$
$$\gamma_{\theta z}^{(0)}=\varphi_2+\frac{1}{R}\frac{\partial w}{\partial \theta}$$

$$k_{xx}^{(1)}=\frac{\partial \varphi_1}{\partial x},\qquad k_{\theta\theta}^{(1)}=\frac{1}{R}\frac{\partial \varphi_2}{\partial \theta},$$
$$k_{x\theta}^{(1)}=\frac{1}{R}\frac{\partial \varphi_1}{\partial \theta}+\frac{\partial \varphi_2}{\partial x}, \tag{A-1}$$

$$k_{xz}^{(2)}=-\left(\varphi_1+\frac{\partial w}{\partial x}\right),\qquad k_{\theta z}^{(2)}=-\left(\varphi_2+\frac{1}{R}\frac{\partial w}{\partial \theta}\right)$$

$$k_{xx}^{(3)}=-\left(\frac{\partial \varphi_1}{\partial x}+\frac{\partial^2 w}{\partial x^2}\right),$$
$$k_{\theta\theta}^{(3)}=-\frac{1}{R}\left(\frac{\partial \varphi_2}{\partial \theta}+\frac{1}{R}\frac{\partial^2 w}{\partial \theta^2}\right),$$
$$k_{x\theta}^{(3)}=-\left(\frac{1}{R}\frac{\partial \varphi_1}{\partial \theta}+\frac{2}{R}\frac{\partial^2 w}{\partial x\partial \theta}+\frac{\partial \varphi_2}{\partial x}\right)$$

Appendix B

The non-zero arrays of [K], [M] and [C] matrices are as follows:

$$K_{11}=-Q_{110}P_n^{\,2}-\frac{Q_{660}\beta_m^{\,2}}{R^2}, \tag{B-1}$$

$$K_{12}=-\frac{1}{R}\left(P_nQ_{120}\beta_m+P_nQ_{660}\beta_m\right), \tag{B-2}$$

$$K_{13}=c_1Q_{113}P_n^{\,3}+\frac{c_1Q_{123}\beta_m^{\,2}P_n}{R^2}+\frac{1}{R}Q_{120}P_n+2\frac{c_1Q_{663}\beta_m^{\,2}P_n}{R^2}, \tag{B-3}$$

$$K_{14}=-Q_{111}P_n^{\,2}+c_1Q_{113}P_n^{\,2}-\frac{Q_{661}\beta_m^{\,2}}{R^2}+\frac{c_1Q_{663}\beta_m^{\,2}}{R^2}, \tag{B-4}$$

$$K_{15}=-\frac{1}{R}\begin{pmatrix}-P_nQ_{123}c_1\beta_m-P_nQ_{663}\beta_mc_1\\+P_nQ_{121}\beta_m+P_nQ_{661}\beta_m\end{pmatrix}, \tag{B-5}$$

$$K_{16}=F_{310}P_n, \tag{B-6}$$

$$K_{17}=Y_{310}P_n, \tag{B-7}$$

$$K_{21}=-\frac{1}{R}\left(P_nQ_{210}\beta_m+P_nQ_{660}\beta_m\right), \tag{B-8}$$

$$K_{22}=-\frac{Q_{220}\beta_m^{\,2}}{R^2}-Q_{660}P_n^{\,2}, \tag{B-9}$$

$$K_{23}=2\frac{Q_{663}c_1\beta_mP_n^{\,2}}{R}+\frac{Q_{213}c_1\beta_mP_n^{\,2}}{R}+\frac{Q_{223}c_1\beta_m^{\,3}}{R^3}+\frac{Q_{220}\beta_m}{R^2}, \tag{B-10}$$

$$K_{24}=\frac{1}{R}\begin{pmatrix}P_nQ_{213}\beta_mc_1+P_nQ_{663}\beta_mc_1\\-P_nQ_{211}\beta_m-P_nQ_{661}\beta_m\end{pmatrix}, \tag{B-11}$$

$$K_{25}=-Q_{661}P_n^{\,2}+Q_{663}c_1P_n^{\,2}-\frac{Q_{221}\beta_m^{\,2}}{R^2}+\frac{Q_{223}c_1\beta_m^{\,2}}{R^2}, \tag{B-12}$$

$$K_{26}=\frac{1}{R}F_{320}\beta_m, \tag{B-13}$$

$$K_{27}=\frac{1}{R}Y_{320}\beta_m, \tag{B-14}$$

$$K_{31}=\frac{c_1Q_{213}\beta_m^{\,2}P_n}{R^2}+2\frac{c_1Q_{663}\beta_m^{\,2}P_n}{R^2}+\frac{1}{R}Q_{210}P_n+c_1Q_{113}P_n^{\,3}, \tag{B-15}$$

$$K_{32}=\frac{Q_{223}c_1\beta_m^{\,3}}{R^3}+\frac{Q_{220}\beta_m}{R^2}+\frac{c_1Q_{123}\beta_mP_n^{\,2}}{R}+2\frac{Q_{663}c_1\beta_mP_n^{\,2}}{R}, \tag{B-16}$$

$$K_{33} = -\frac{c_1^2 Q_{226}\beta_m^4}{R^4} - \frac{c_1 Q_{123} P_n^2}{R} - \frac{Q_{213} c_1 P_n^2}{R} - 9\frac{c_1^2 Q_{444}\beta_m^2}{R^2} - 2\frac{Q_{223} c_1 \beta_m^2}{R^3} + 6\frac{Q_{442} c_1 \beta_m^2}{R^2} - Q_{550} P_n^2 - \frac{Q_{220}}{R^2} - Q_{116} c_1^2 P_n^4 - \frac{Q_{126} c_1^2 \beta_m^2 P_n^2}{R^2} - 4\frac{c_1^2 Q_{666}\beta_m^2 P_n^2}{R^2} - \frac{c_1^2 Q_{216}\beta_m^2 P_n^2}{R^2} + 6Q_{552} c_1 P_n^2 - \frac{Q_{440}\beta_m^2}{R^2} - 9Q_{554} c_1^2 P_n^2, \quad \text{(B-17)}$$

$$K_{34} = -\frac{Q_{213} c_1 P_n}{R} - Q_{550} P_n + c_1 Q_{114} P_n^3 - Q_{116} c_1^2 P_n^3 + 2\frac{c_1 Q_{664}\beta_m^2 P_n}{R^2} - 2\frac{c_1^2 Q_{666}\beta_m^2 P_n}{R^2} + \frac{c_1 Q_{214}\beta_m^2 P_n}{R^2} - \frac{c_1^2 Q_{216}\beta_m^2 P_n}{R^2} + 6Q_{552} c_1 P_n - 9Q_{554} c_1^2 P_n + \frac{Q_{211} P_n}{R}, \quad \text{(B-18)}$$

$$K_{35} = -9\frac{c_1^2 Q_{444}\beta_m}{R} + \frac{c_1 Q_{224}\beta_m^3}{R^3} + 6\frac{Q_{442} c_1 \beta_m}{R} - \frac{c_1^2 Q_{226}\beta_m^3}{R^3} - \frac{Q_{223} c_1 \beta_m}{R^2} + \frac{Q_{221}\beta_m}{R^2} + \frac{c_1 Q_{124}\beta_m P_n^2}{R} - \frac{Q_{126} c_1^2 \beta_m P_n^2}{R} + 2\frac{c_1 Q_{664}\beta_m P_n^2}{R} - 2\frac{c_1^2 Q_{666}\beta_m P_n^2}{R} - \frac{Q_{440}\beta_m}{R}, \quad \text{(B-19)}$$

$$K_{36} = -\frac{c_1 F_{323}\beta_m^2}{R^2} - 3\frac{c_1 F_{242}\beta_m^2}{R} + F_{150} P_n^2 - \frac{F_{320}}{R} - c_1 F_{313} P_n^2 + \frac{F_{240}\beta_m^2}{R} - 3c_1 F_{152} P_n^2, \quad \text{(B-20)}$$

$$K_{37} = -3\frac{c_1 Y_{242}\beta_m^2}{R} - \frac{c_1 Y_{323}\beta_m^2}{R^2} + Y_{150} P_n^2 - \frac{Y_{320}}{R} - c_1 Y_{313} P_n^2 + \frac{Y_{240}\beta_m^2}{R} - 3c_1 Y_{152} P_n^2, \quad \text{(B-21)}$$

$$K_{41} = -Q_{111} P_n^2 + Q_{113} c_1 P_n^2 - \frac{Q_{661}\beta_m^2}{R^2} + \frac{Q_{663} c_1 \beta_m^2}{R^2}, \quad \text{(B-22)}$$

$$K_{42} = -\frac{Q_{121}\beta_m P_n}{R} + \frac{Q_{123} c_1 \beta_m P_n}{R} - \frac{Q_{661}\beta_m P_n}{R} + \frac{Q_{663} c_1 \beta_m P_n}{R}, \quad \text{(B-23)}$$

$$K_{43} = -\frac{c_1 Q_{123} P_n}{R} - Q_{550} P_n + \frac{Q_{121} P_n}{R} + c_1 Q_{114} P_n^3 - 9Q_{554} c_1^2 P_n - Q_{116} c_1^2 P_n^3 + 6Q_{552} c_1 P_n + \frac{Q_{124} c_1 \beta_m^2 P_n}{R^2} - 2\frac{c_1^2 Q_{666}\beta_m^2 P_n}{R^2} + 2\frac{c_1 Q_{664}\beta_m^2 P_n}{R^2} - \frac{Q_{126} c_1^2 \beta_m^2 P_n}{R^2}, \quad \text{(B-24)}$$

$$K_{44} = -\frac{c_1^2 Q_{666}\beta_m^2}{R^2} + 2\frac{c_1 Q_{664}\beta_m^2}{R^2} - Q_{550} - 9Q_{554} c_1^2 + 6Q_{552} c_1 - Q_{112} P_n^2 + 2Q_{114} c_1 P_n^2 - \frac{Q_{662}\beta_m^2}{R^2} - Q_{116} c_1^2 P_n^2, \quad \text{(B-25)}$$

$$K_{45} = -\frac{Q_{662}\beta_m P_n}{R} - \frac{Q_{122}\beta_m P_n}{R} + 2\frac{Q_{124} c_1 \beta_m P_n}{R} + 2\frac{c_1 Q_{664}\beta_m P_n}{R} - \frac{c_1^2 Q_{666}\beta_m P_n}{R} - \frac{Q_{126} c_1^2 \beta_m P_n}{R}, \quad \text{(B-26)}$$

$$K_{46} = -3F_{152} P_n c_1 - F_{313} P_n c_1 + F_{150} P_n + F_{311} P_n, \quad \text{(B-27)}$$

$$K_{47} = -3P_n Y_{152} c_1 - P_n Y_{313} c_1 + P_n Y_{150} + P_n Y_{311}, \quad \text{(B-28)}$$

$$K_{51} = -\frac{Q_{661}\beta_m P_n}{R} + \frac{Q_{663} c_1 \beta_m P_n}{R} - \frac{Q_{211}\beta_m P_n}{R} + \frac{Q_{213} c_1 \beta_m P_n}{R}, \quad \text{(B-29)}$$

$$K_{52} = -Q_{661} P_n^2 + Q_{663} c_1 P_n^2 - \frac{Q_{221}\beta_m^2}{R^2} + \frac{Q_{223} c_1 \beta_m^2}{R^2}, \quad \text{(B-30)}$$

$$K_{53} = -\frac{Q_{223}c_1\beta_m}{R^2} + \frac{c_1 Q_{224}\beta_m{}^3}{R^3} - 9\frac{c_1{}^2 Q_{444}\beta_m}{R} - \frac{c_1{}^2 Q_{226}\beta_m{}^3}{R^3} + 6\frac{Q_{442}c_1\beta_m}{R} - \frac{c_1{}^2 Q_{216}\beta_m P_n{}^2}{R} + \frac{Q_{214}c_1\beta_m P_n{}^2}{R} - 2\frac{c_1{}^2 Q_{666}\beta_m P_n{}^2}{R} + 2\frac{c_1 Q_{664}\beta_m P_n{}^2}{R} + \frac{Q_{221}\beta_m}{R^2} - \frac{Q_{440}\beta_m}{R}, \tag{B-31}$$

$$K_{54} = -\frac{Q_{212}\beta_m P_n}{R} - \frac{Q_{662}\beta_m P_n}{R} + 2\frac{c_1 Q_{214}\beta_m P_n}{R} - \frac{c_1{}^2 Q_{216}\beta_m P_n}{R} - \frac{c_1{}^2 Q_{666}\beta_m P_n}{R} + 2\frac{c_1 Q_{664}\beta_m P_n}{R}, \tag{B-32}$$

$$K_{55} = -9c_1{}^2 Q_{444} - Q_{662}P_n{}^2 + 6Q_{442}c_1 - \frac{c_1{}^2 Q_{226}\beta_m{}^2}{R^2} + 2\frac{c_1 Q_{224}\beta_m{}^2}{R^2} - Q_{440} + 2Q_{664}c_1 P_n{}^2 - \frac{Q_{222}\beta_m{}^2}{R^2} - Q_{666}c_1{}^2 P_n{}^2, \tag{B-33}$$

$$K_{56} = F_{240}\beta_m - \frac{F_{323}c_1\beta_m}{R} + \frac{F_{321}\beta_m}{R} - 3c_1 F_{242}\beta_m, \tag{B-34}$$

$$K_{57} = Y_{240}\beta_m - \frac{c_1 Y_{323}\beta_m}{R} + \frac{Y_{321}\beta_m}{R} - 3c_1 Y_{242}\beta_m, \tag{B-35}$$

$$K_{61} = -F_{310}P_n, \tag{B-36}$$

$$K_{62} = -\frac{F_{320}\beta_m}{R}, \tag{B-37}$$

$$K_{63} = c_1 F_{313}P_n{}^2 + \frac{c_1 F_{323}\beta_m{}^2}{R^2} + \frac{F_{320}}{R} + 3c_1 F_{152}P_n{}^2 - F_{150}P_n{}^2 + 3\frac{F_{242}c_1\beta_m{}^2}{R^2} - \frac{F_{240}\beta_m{}^2}{R^2}, \tag{B-38}$$

$$K_{64} = 3F_{152}P_n c_1 + F_{313}P_n c_1 - F_{150}P_n - F_{311}P_n, \tag{B-39}$$

$$K_{65} = -\frac{F_{321}\beta_m}{R} + \frac{F_{323}c_1\beta_m}{R} - \frac{F_{240}\beta_m}{R} + 3\frac{c_1 F_{242}\beta_m}{R}, \tag{B-40}$$

$$K_{66} = -\frac{U_{220}\beta_m{}^2}{R^2} - U_{110}P_n{}^2 - U_{330}, \tag{B-41}$$

$$K_{67} = -\frac{X_{220}\beta_m{}^2}{R^2} - X_{110}P_n{}^2 - X_{330}, \tag{B-42}$$

$$K_{71} = -Y_{310}P_n, \tag{B-43}$$

$$K_{72} = -\frac{Y_{320}\beta_m}{R}, \tag{B-44}$$

$$K_{73} = c_1 Y_{313}P_n{}^2 + \frac{c_1 Y_{323}\beta_m{}^2}{R^2} + \frac{Y_{320}}{R} + 3c_1 Y_{152}P_n{}^2 - Y_{150}P_n{}^2 + 3\frac{Y_{242}c_1\beta_m{}^2}{R^2} - \frac{Y_{240}\beta_m{}^2}{R^2}, \tag{B-45}$$

$$K_{74} = 3P_n Y_{152}c_1 + P_n Y_{313}c_1 - P_n Y_{150} - P_n Y_{311}, \tag{B-46}$$

$$K_{75} = -\frac{Y_{321}\beta_m}{R} + \frac{c_1 Y_{323}\beta_m}{R} - \frac{Y_{240}\beta_m}{R} + 3\frac{c_1 Y_{242}\beta_m}{R}, \tag{B-47}$$

$$K_{76} = -\frac{X_{220}\beta_m{}^2}{R^2} - X_{110}P_n{}^2 - X_{330}, \tag{B-48}$$

$$K_{77} = -\frac{L_{220}\beta_m{}^2}{R^2} - L_{110}P_n{}^2 - L_{330}, \tag{B-49}$$

$$M_{11} = I_0, \tag{B-50}$$

$$M_{13} = -I_3 P_n c_1, \tag{B-51}$$

$$M_{14} = -I_3 c_1 + I_1, \tag{B-52}$$

$$M_{22} = I_0, \tag{B-53}$$

$$M_{23} = -\frac{1}{R}I_3 c_1\beta_m, \tag{B-54}$$

$$M_{25} = -I_3 c_1 + I_1, \tag{B-55}$$

$$M_{31} = -I_3 c_1 P_n, \tag{B-56}$$

$$M_{32} = -\frac{1}{R} I_3 c_1 \beta_m, \tag{B-57}$$

$$M_{33} = I_6 {c_1}^2 {P_n}^2 + \frac{I_6 {c_1}^2 {\beta_m}^2}{R^2} + I_0, \tag{B-58}$$

$$M_{34} = I_6 P_n c_1^2 - I_4 P_n c_1, \tag{B-59}$$

$$M_{35} = \frac{1}{R}\left(-I_4 c_1 \beta_m + I_6 c_1^2 \beta_m\right), \tag{B-60}$$

$$M_{41} = -I_3 c_1 + I_1, \tag{B-61}$$

$$M_{43} = I_6 P_n c_1^2 - I_4 P_n c_1, \tag{B-62}$$

$$M_{44} = I_6 c_1^2 - 2I_4 c_1 + I_2, \tag{B-63}$$

$$M_{52} = -I_3 c_1 + I_1, \tag{B-64}$$

$$M_{53} = \frac{1}{R}\left(-I_4 c_1 \beta_m + I_6 c_1^2 \beta_m\right), \tag{B-65}$$

$$M_{55} = I_6 c_1^2 - 2I_4 c_1 + I_2, \tag{B-66}$$

$$C_{33} = C_d \tag{B-67}$$

The used coefficients in “Appendix B” are defined as follows:

$$Q_{ijk} = \int_z Q_{ij}\, z^k \,\mathrm{d}z, \qquad i, j = 1, 2, ..., 6 \tag{B-68}$$

$$F_{15k} = \int_z e_{15} \cos\left(\frac{\pi z}{h}\right) z^k \,\mathrm{d}z, \qquad k = 0, 2 \tag{B-69}$$

$$F_{24k} = \int_z e_{24} \cos\left(\frac{\pi z}{h}\right) z^k \,\mathrm{d}z, \qquad k = 0, 1, 2, 3 \tag{B-70}$$

$$F_{3jk} = \int_z e_{3j} \left[\frac{\pi}{h}\right] \sin\left(\frac{\pi z}{h}\right) z^k \,\mathrm{d}z,\ j = 1, 2,\ k = 0, 1, 3 \tag{B-71}$$

$$U_{ii0} = \int_z s_{ii} \cos^2\left(\frac{\pi z}{h}\right) \mathrm{d}z, \qquad i = 1, 2 \tag{B-72}$$

$$U_{330} = \int_z s_{33} \left[\frac{\pi^2}{h^2}\right] \sin^2\left(\frac{\pi z}{h}\right) \mathrm{d}z, \tag{B-73}$$

$$U_{333} = \int_z s_{33} \left[\frac{\pi}{h^2}\right] \sin\left(\frac{\pi z}{h}\right) \mathrm{d}z, \tag{B-74}$$

$$Y_{15k} = \int_z q_{15} \cos\left(\frac{\pi z}{h}\right) z^k \,\mathrm{d}z, \qquad k = 0, 2 \tag{B-75}$$

$$Y_{24k} = \int_z q_{24} \cos\left(\frac{\pi z}{h}\right) z^k \,\mathrm{d}z, \qquad k = 0, 1, 2, 3 \tag{B-76}$$

$$Y_{3jk} = \int_z q_{3j} \left[\frac{\pi}{h}\right] \sin\left(\frac{\pi z}{h}\right) z^k \,\mathrm{d}z,\ j = 1, 2,\ k = 0, 1, 3 \tag{B-77}$$

$$L_{ii0} = \int_z \mu_{ii} \cos^2\left(\frac{\pi z}{h}\right) \mathrm{d}z, \qquad i = 1, 2 \tag{B-78}$$

$$L_{330} = \int_z \mu_{33} \left[\frac{\pi^2}{h^2}\right] \sin^2\left(\frac{\pi z}{h}\right) \mathrm{d}z, \tag{B-79}$$

$$L_{333} = \int_z \mu_{33} \left[\frac{\pi}{h^2}\right] \sin\left(\frac{\pi z}{h}\right) \mathrm{d}z, \tag{B-80}$$

$$X_{ii0} = \int_z d_{ii} \cos^2\left(\frac{\pi z}{h}\right) \mathrm{d}z, \qquad i = 1, 2 \tag{B-81}$$

$$X_{330} = \int_z d_{33} \left[\frac{\pi^2}{h^2}\right] \sin^2\left(\frac{\pi z}{h}\right) \mathrm{d}z, \tag{B-82}$$

$$X_{333} = \int_z d_{33} \left[\frac{\pi}{h^2}\right] \sin\left(\frac{\pi z}{h}\right) \mathrm{d}z \tag{B-83}$$